

MAXIMUM TORQUE PER AMPERE CONTROL OF INTERIOR PERMANENT MAGNET
SYNCHRONOUS MOTOR VIA OPTIMAL CURRENT EXCITATION

by

Taowen Chen



APPROVED BY SUPERVISORY COMMITTEE:

Dr. Babak Fahimi, Chair

Dr. Bilal Akin

Dr. Poras T. Balsara

Dr. Ghanshyamsinh Gohil

Copyright 2019

Taowen Chen

All Rights Reserved

MAXIMUM TORQUE PER AMPERE CONTROL OF INTERIOR PERMANENT MAGNET
SYNCHRONOUS MOTOR VIA OPTIMAL CURRENT EXCITATION

by

TAOWEN CHEN, BS

THESIS

Presented to the Faculty of
The University of Texas at Dallas
in Partial Fulfillment
of the Requirements
for the Degree of

MASTER OF SCIENCE IN
ELECTRICAL ENGINEERING

THE UNIVERSITY OF TEXAS AT DALLAS

May 2019

ACKNOWLEDGMENTS

I would like to express my sincere gratitude to my supervisor, Dr. Babak Fahimi for providing the opportunity of working as a student worker at Renewable Energy and Vehicular Technology Laboratory (REVT). The encouragement and guidance from Dr. Fahimi helped me achieve the goal of my research, and the experience I gained in the lab serves to polish my skills both professionally and academically.

I want to thank Dr. Bilal Akin, Dr. Poras T. Balsara and Dr. Ghanshyamsinh Gohil for serving on my committee. I also would like to extend my appreciation to my colleagues in the REVT lab, their technical and intellectual help has been so supportive and inspiring throughout my research in the lab, especially Dingyi He, Jingchen Liang and Carlos Caicedo-Narvaez.

Last but not least, I would like to thank my parents, Jianming Chen and Fangmei Min, for all the sacrifice they made to support me as a graduate student here.

March 2019

MAXIMUM TORQUE PER AMPERE CONTROL OF INTERIOR PERMANENT MAGNET SYNCHRONOUS MOTOR VIA OPTIMAL CURRENT EXCITATION

Taowen Chen, MS
The University of Texas at Dallas, 2019

Supervising Professor: Dr. Babak Fahimi

This research focuses on the optimal current excitation of interior permanent magnet synchronous motors (IPMSM) with non-sinusoidal back electromotive-force (BEMF) for maximum torque per ampere (MTPA) control. In this thesis, an analytical expression for average torque in IPMSM as well as a closed form for optimal current excitation are presented, the optimal current is presented as a function of each current harmonics with different magnitude and frequency to render a better understanding of torque generation in IPMSM, hysteresis current control has been used for current injection in IPMSM, prototype development and testing process have been discussed, validation through both simulation and experimental results with detailed analysis are provided.

TABLE OF CONTENTS

ACKNOWLEDGMENTS	iv
TABLE OF CONTENTS.....	vi
LIST OF FIGURES	vii
LIST OF TABLES	x
CHAPTER 1 INTRODUCTION	1
1.1 Background	1
1.2 Literature review	2
1.3 Objective of Thesis	5
1.4 Organization of Thesis	6
CHAPTER 2 MTPA CONTROL IN IPMSM.....	7
2.1 Basic Model of IPMSM	7
2.2 Average Torque Derivation in IPMSM	8
2.3 Maximum Torque per Ampere Solution for IPMSM	13
2.4 Summary	15
CHAPTER 3 SIMULATION RESULTS ANALYSIS	16
3.1 Model Analysis	16
3.2 Current Injection Method.....	22
3.3 Summary	34
CHAPTER 4 EXPERIMENTAL IMPLEMENTATION	35
4.1 Testbed Introduction	35
4.2 Hardware Implementation	35
4.3 Experimental Results	43
CHAPTER 5 CONCLUSION AND SUGGESTED FUTURE WORK.....	51
5.1 Conclusion	51
5.2 Suggested Future work	51
REFERENCES	52
BIOGRAPHICAL SKETCH	55
CURRICULUM VITAE	56

LIST OF FIGURES

Figure 1.1. (a) Surface-Mounted PMSM (b) Interior PMSM.....	2
Figure 1.2. Projection from abc to dq	3
Figure 1.3. Modified Inverter Topology	5
Figure 3.1. 2D model of IPMSM	16
Figure 3.2. BEMF of IPMSM	17
Figure 3.3. Flux Linkage of IPMSM	17
Figure 3.4. FFT Analysis Flux Linkage of IPMSM.....	18
Figure 3.5. Normalized Current Waveform.....	20
Figure 3.6. Torque Profile of Sinusoidal Current Excitation.....	20
Figure 3.7. Torque Profile of Optimal Current Excitation.....	21
Figure 3.8. Torque Profile of Optimal Current Excitation.....	21
Figure 3.9. Pure Sinusoidal Three-Phase Current and Two-Phase current.....	23
Figure 3.10. Harmonics in dq abc Frame and FFT analysis	24
Figure 3.11. Control Scheme of Phase Current	25
Figure 3.12. Bode Plot of the Open Loop system.....	26
Figure 3.13. Step Response.....	27
Figure 3.14. Bode Plot of Close Loop System.....	27
Figure 3.15. Input Signal with Frequency of 10 Hz	28
Figure 3.16. Input Signal with Frequency of 90 Hz	28
Figure 3.17. Three-phase Inverter Connected to Load	29
Figure 3.18. Hysteresis Control and Switching Action of S1	30

Figure 3.19. Three-phase Inverter with RL Load	31
Figure 3.20. Control Logic of Switches.....	31
Figure 3.21. First Order Current and Third Order Current	32
Figure 3.22. FFT Analysis	32
Figure 3.23. First Order Current and Fifth Order Current	33
Figure 3.24. FFT Analysis	33
Figure 4.1. IPMSM Control Testbed	36
Figure 4.2. Control Scheme of IPMSM	36
Figure 4.3. (a) Top of PCB (b) Bottom of PCB.....	37
Figure 4.4. Isolated Power Supply Design.....	38
Figure 4.5. Experimental Results of Designed Isolated Power Supply	39
Figure 4.6. Design of Bootstrap Circuit for Three-phase Inverter.....	40
Figure 4.7. Voltage of Bootstrap Capacitor	41
Figure 4.8. Current Sensing Circuit	42
Figure 4.9. Phase Current of 1A	43
Figure 4.10. Measured BEMF of IPMSM	44
Figure 4.11. Simulated and Measured BEMF	44
Figure 4.12. Sinusoidal Current at 2.2A PEAK.....	45
Figure 4.13. Optimal Current at 2.2A PEAK.....	46
Figure 4.14. Measured Torque and FFT Analysis at 2.2A PEAK.....	47
Figure 4.15. Sinusoidal Current at 3A PEAK.....	48
Figure 4.16. Optimal Current at 3A PEAK.....	48

Figure 4.17. Measured Torque and FFT Analysis at 3A PEAK.....	49
Figure 4.18. Comparison of TPA Improvement	50

LIST OF TABLES

Table 1. Magnitude of Current Harmonics(Peak).....	19
Table 2. Simulation and Numerical Calculation Result of Torque Improvement	22
Table 3. Relation Between Three-phase and Two-phase Harmonics	24
Table 4. Performance of the step response	26
Table 5. Voltage Levels of Hardware	35
Table 6. Experimental Implementation Details	42
Table 7. Experimental Results Analysis	49

CHAPTER 1

INTRODUCTION

1.1 Background

Among different types of electric motors, permanent magnet synchronous motors (PMSM) are popular due to high-power density, high-torque-to-inertia ratio, and wide speed range in constant power region [1]. With the existence of the permanent magnet, the requirement of rotor current for rotor field generation can be eliminated, which ensures a higher efficiency operation. Brushless operations free this type of motor from the high maintenance cost and the price of the brushes, there are lots of applications where PMSMs plays an important role such as air-conditioner compressor, electric vehicles, home appliances etc.

PMSMs are divided into two main categories (shown in Figure 1.1 (a) and (b)) based on the location of the permanent magnet on the rotor, one of these is the surface-mounted permanent magnet synchronous motor (SPMSM), magnets are attached on the surface of the rotor. The other one is the interior permanent magnet motor (IPMSM), in which the magnets are buried inside the rotor, the buried structure makes IPMSM robust for high speed application, however, this will also cause the IPMSM to exhibit magnetic saliency in $dq0$ reference frame[2], since the permanent magnets are buried in the d-axis, the inductance in q-axis is larger than that in d-axis, the difference in inductances between d-axis and q-axis contributes to an additional torque component, reluctance torque.

The torque generated in IPMSM is comprised of two components, the electromagnetic torque and the reluctance torque, the former one is proportional to the q-axis current, and the latter one is proportional to the product of product of d-axis and q-axis current, so, different current vectors

can be selected to produce the same amount of torque. Among these current vectors, the one with the minimum magnitude is called the maximum torque per ampere (MTPA) current[3].

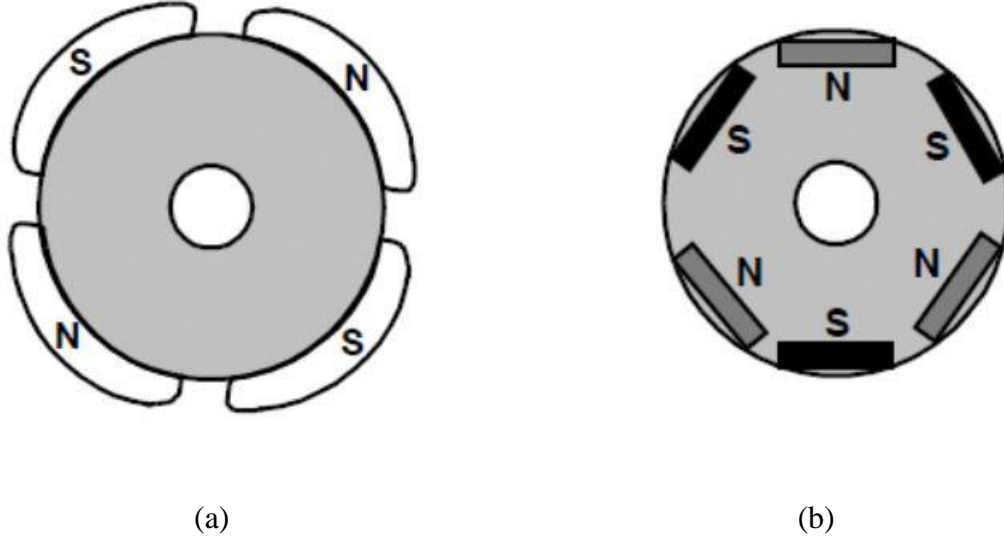


Figure 1.1. (a) Surface-Mounted PMSM (b) Interior PMSM

1.2 Literature review

1.2.1 PMSM Control

The phase voltage and current in PMSM can be represented as following

$$[F_a \quad F_b \quad F_c]^T = [F_m \cos(\theta) \quad F_m \cos\left(\theta - \frac{2}{3}\pi\right) \quad F_m \cos\left(\theta + \frac{2}{3}\pi\right)]^T \quad (1-1)$$

where F_a , F_b and F_c are the current or voltage components, F_m is the magnitude of those component, θ is the electrical rotor position.

The most popular way for PMSM control is Field-oriented Control (FOC), which focuses on decoupling the three-phase stator currents into a magnetic field generating component and torque generating component. By controlling the two components separately, PMSM can be controlled

like a DC motor. The decoupling consists a projection called abc to $dq0$ transformation (shown in Figure 2), the transformation is presented in equation (1-2)

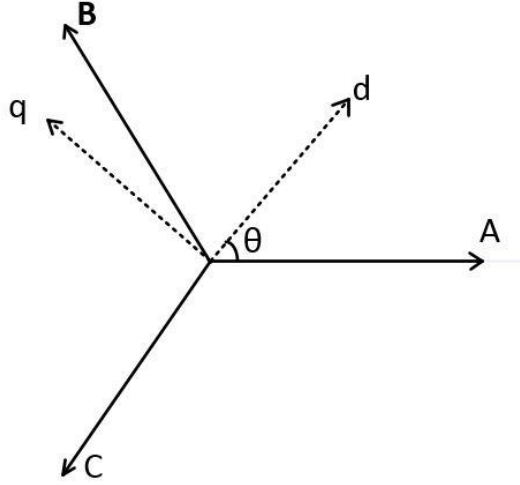


Figure 1.2. Projection from abc to dq

$$\begin{bmatrix} F_d \\ F_q \\ F_0 \end{bmatrix} = \begin{bmatrix} \sin(\theta) & \sin\left(\theta - \frac{2}{3}\pi\right) & \sin\left(\theta + \frac{2}{3}\pi\right) \\ \cos(\theta) & \cos\left(\theta - \frac{2}{3}\pi\right) & \cos\left(\theta + \frac{2}{3}\pi\right) \\ \frac{1}{2} & \frac{1}{2} & \frac{1}{2} \end{bmatrix} \begin{bmatrix} F_a \\ F_b \\ F_c \end{bmatrix} \quad (1 - 2)$$

where F_d and F_q are the vectors projected on direct and quadrature axis. By controlling the components in d-axis and q-axis, PMSM can be controlled.

1.2.2 MTPA Control

Considerable studies have been done on the control of IPMSM in MTPA control, in [4][5][6], the calculation of MTPA point was done by using nominal motor parameters, with a phase angel in the armature current, the MTPA control is achieved, nevertheless, the parameters of the motor might change due to several factors, for example, the temperature will change the value of resistance and permanent magnet flux linkage[7], L_q , the inductance in q-axis, whose value will

also change with different current magnitude and current phase angel[8]. Approaches of on-line motor parameter estimation to compensate the parameter variations have been proposed and validated in reference [9]-[11]. The work mentioned above is based on the relationship between the current in d-axis and q-axis shown in Equation (1-3)

$$i_d = \frac{\phi_M}{2(L_d - L_q)} - \sqrt{\frac{\phi_M^2}{4(L_d - L_q)^2} + i_q^2} \quad (1 - 3)$$

Where ϕ_M is the flux linkage created by the permanent magnet, L_d , L_q are the inductances in $dq0$ frame of reference.

Besides, some researchers focus on the back electromotive-force (BEMF) to find the optimal current for MTPA operation. It is often the case that permanent magnet (PM) motors with sinusoidal back electromotive force (BEMF) are excited by sinusoidal current [12], and PM motors with trapezoidal BEMF are excited with rectangular current [13]. However, the practical BEMF can merely approximate the ideal scenarios mentioned above and more attention should be given to the PM motors with non-sinusoidal BEMF.

Considerable work has been done in the area of optimal current excitation to address the problem mentioned above. In [14]-[16], optimal current was calculated and injected in a surface-mounted permanent magnet synchronous motor to achieve MTPA. In reference [17], [18] and [19], optimal current was fed into the IPMSM and brushless DC (BLDC) motor. In [20], the expression for optimal current was presented as a function of each current harmonic with different magnitude and frequency, this method of calculating optimal current for MTPA not only applies to PMSMs but also synchronous reluctance machine.

Since the optimal current for MTPA control always includes high order current harmonics if the motor exhibits non-sinusoidal BEMF, in [21], optimal current was injected into IPMSM by using vector control, in [22] hysteresis current control was used to construct the optimal current, in [23] and [24], inverter topology has been modified (shown in Figure 3) by adding a fourth branch connecting to the motor neutral point to allow a third-order harmonic current in the system.

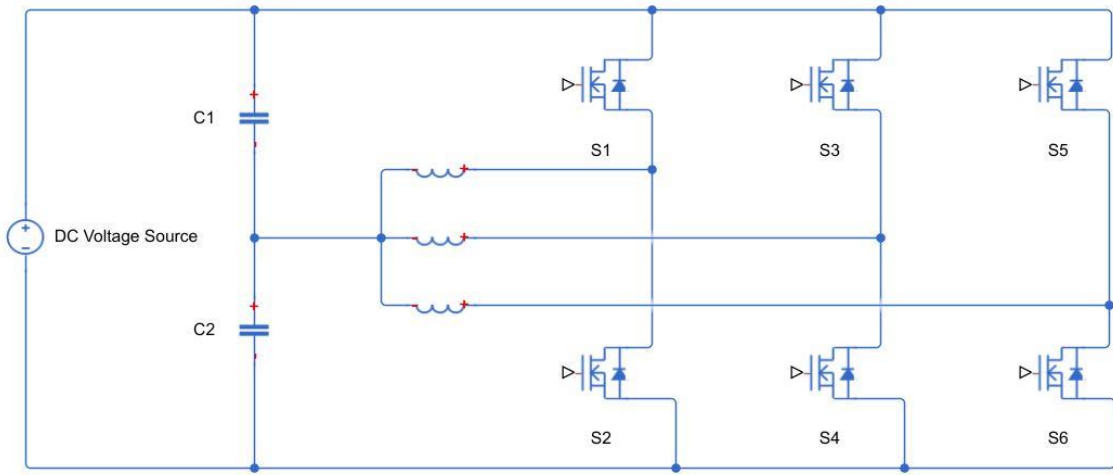


Figure 1.3. Modified Inverter Topology

1.3 Objective of Thesis

Since the saliency of the rotor, an additional reluctance torque exists in the IPMSM, moreover, the traditional way of MTPA control only applies to the case in which IPMSM are exhibiting sinusoidal BEMF, so the higher order current harmonics are ignored in most of the work, the objective of the thesis is to provide a general solution to find the optimal current for MTPA control in IPMSM, rather than using vector control for current harmonic injection, inverter topology in Figure 2 is designed and the hysteresis current control is used for feed the IPMSM with the optimal current.

1.4 Organization of Thesis

The model of IPM and the detailed derivation of optimal current for MTPA control will be presented in Chapter 2. Numerical analysis and case study with Finite Element Analysis (FEA) simulation results in will be discussed to validate the method mentioned in Chapter 3. Experimental setup description and some procedures for implementation the MTPA control will be discussed in Chapter 4. Conclusion is given in Chapter 5.

CHAPTER 2

MTPA CONTROL IN IPMSM

2.1 Basic Model of IPMSM

IPMSM can be modeled in a 3-phase frame of reference, assuming the leakage inductance is neglected, and the electrical angle between d-axis and phase A is defined as rotor electrical position θ , the phase inductance can be considered as a function of rotor electrical position θ , since the reluctance of the rotor change with rotor position, according to [2], the phase self-inductance can be expressed as following:

$$L_a(\theta) = L_A - L_B \cos 2(\theta) \quad (2-1)$$

$$L_b(\theta) = L_A - L_B \cos 2\left(\theta - \frac{\pi}{3}\right) \quad (2-2)$$

$$L_c(\theta) = L_A - L_B \cos 2\left(\theta + \frac{\pi}{3}\right) \quad (2-3)$$

the mutual inductances between different phases can be expressed as:

$$L_{ab}(\theta) = -\frac{1}{2}L_A - L_B \cos 2\left(\theta - \frac{2\pi}{3}\right) \quad (2-4)$$

$$L_{ca}(\theta) = -\frac{1}{2}L_A - L_B \cos 2\left(\theta + \frac{2\pi}{3}\right) \quad (2-5)$$

$$L_{bc}(\theta) = -\frac{1}{2}L_A - L_B \cos 2(\theta) \quad (2-6)$$

The flux produced by the permanent magnet is shown as:

$$\phi_a(\theta) = \phi_m \cos(\theta) \quad (2-7)$$

$$\phi_b(\theta) = \phi_m \cos\left(\theta - \frac{2\pi}{3}\right) \quad (2-8)$$

$$\phi_c(\theta) = \phi_m \cos\left(\theta + \frac{2\pi}{3}\right) \quad (2-9)$$

the motor equation can be written in a three-phase model shown in 2-10.

$$\begin{bmatrix} v_a \\ v_b \\ v_c \end{bmatrix} = \begin{bmatrix} R_a & 0 & 0 \\ 0 & R_b & 0 \\ 0 & 0 & R_c \end{bmatrix} \begin{bmatrix} i_a \\ i_b \\ i_c \end{bmatrix} + \frac{d}{dt} \begin{bmatrix} L_a(\theta r) & L_{ab}(\theta r) & L_{ca}(\theta r) \\ L_{ab}(\theta r) & L_b(\theta r) & L_{bc}(\theta r) \\ L_{ca}(\theta r) & L_{bc}(\theta r) & L_c(\theta r) \end{bmatrix} \begin{bmatrix} i_a \\ i_b \\ i_c \end{bmatrix} + \frac{d}{dt} \begin{bmatrix} \phi_a(\theta r) \\ \phi_b(\theta r) \\ \phi_c(\theta r) \end{bmatrix} \quad (2-10)$$

2.2 Average Torque Derivation in IPMSM

Due to the structure of the IPMSM, permanent magnets are buried inside the rotor, thereby introducing a saliency to the motor and furthermore creating reluctance torque in IPMSM. Thus, the total output torque of IPMSM consists of two parts, the electromagnetic reaction torque and the reluctance torque. The BEMF and flux linkage of the IPMSM can be presented by the following Fourier series

$$E_a(\theta) = \sum_{-\infty}^{+\infty} E_k \cos k(\theta) \quad (2-11)$$

$$E_b(\theta) = \sum_{-\infty}^{+\infty} E_k \cos k\left(\theta - \frac{2\pi}{3}\right) \quad (2-12)$$

$$E_c(\theta) = \sum_{-\infty}^{+\infty} E_k \cos k\left(\theta - \frac{2\pi}{3}\right) \quad (2-13)$$

$$\lambda_a(\theta) = \sum_{-\infty}^{+\infty} \lambda_k \sin k(\theta) \quad (2-14)$$

$$\lambda_b(\theta) = \sum_{-\infty}^{+\infty} \lambda_k \sin k\left(\theta - \frac{2\pi}{3}\right) \quad (2-15)$$

$$\lambda_c(\theta) = \sum_{-\infty}^{+\infty} \lambda_k \sin k \left(\theta - \frac{2\pi}{3} \right) \quad (2-16)$$

According to [20], the phase current can be presented as

$$I_a(\theta) = \sum_{-\infty}^{+\infty} [I_{\alpha k} \cos k(\theta) + I_{\beta k} \sin k(\theta)] \quad (2-17)$$

$$I_b(\theta) = \sum_{-\infty}^{+\infty} [I_{\alpha k} \cos k \left(\theta - \frac{2}{3}\pi \right) + I_{\beta k} \sin k \left(\theta - \frac{2}{3}\pi \right)] \quad (2-18)$$

$$I_c(\theta) = \sum_{-\infty}^{+\infty} [I_{\alpha k} \cos k \left(\theta + \frac{2}{3}\pi \right) + I_{\beta k} \sin k \left(\theta + \frac{2}{3}\pi \right)] \quad (2-19)$$

In which E_k , λ_k , $I_{\alpha k}$ and $I_{\beta k}$ are the Fourier coefficients of k th order harmonic.

The average electromagnetic torque (only two-pole machine is considered here) over one electrical cycle is given by:

$$\begin{aligned} T_{ave} &= \frac{1}{2\pi w_m} \int_0^{2\pi} E_a(\theta) I_a(\theta) + E_b(\theta) I_b(\theta) + E_c(\theta) I_c(\theta) d\theta \\ &= \frac{3}{2\pi w_m} \int_0^{2\pi} \frac{d\lambda_k(\theta)}{dt} I_a(\theta) d\theta \\ &= \frac{3}{2\pi w_m} \int_0^{2\pi} \frac{d\lambda_k(\theta)}{d\theta} \frac{d\theta}{dt} I_a(\theta) d\theta \\ &= \frac{3}{2\pi w_m} \int_0^{2\pi} \frac{d\lambda_k(\theta)}{d\theta} w_m I_a(\theta) d\theta \\ &= \frac{3}{2\pi} \int_0^{2\pi} I_a(\theta) d\lambda_k(\theta) \\ &= \sum_{-\infty}^{+\infty} \frac{3}{2\pi} \int_0^{2\pi} I_{\alpha k} \lambda_k \cos k(\theta) \cos k(\theta) d k \theta \\ &= \frac{3}{2} \sum_{-\infty}^{+\infty} I_{\alpha k} \lambda_k \end{aligned} \quad (2-20)$$

Where w_m is the rotor mechanical speed. From Equation 2-20, it can be observed that all the harmonics in flux linkage (or BEMF) contribute to the average torque production.

The average reluctance torque [25] is expressed by

$$T_{rel} = \frac{1}{2}I_a(\theta)^2 \frac{dL_a(\theta)}{d\theta} + \frac{1}{2}I_b(\theta)^2 \frac{dL_b(\theta)}{d\theta} + \frac{1}{2}I_c(\theta)^2 \frac{dL_c(\theta)}{d\theta} + I_a(\theta)I_b(\theta) \frac{dL_{ab}(\theta)}{d\theta} + I_b(\theta)I_c(\theta) \frac{dL_{bc}(\theta)}{d\theta} + I_c(\theta)I_a(\theta) \frac{dL_{ca}(\theta)}{d\theta} \quad (2-21)$$

By plugging in the Equation (2-1) to (2-6) and (2-14) to (2-16) into (2-21), the following torque equation (2-22) is obtained. The reluctance torque can be separated into two parts, one is the torque component from self-inductance, and another part comes from mutual-inductance [20].

$$T_{rel} = (I_a(\theta)^2 + 2I_b(\theta)I_c(\theta))L_B \sin 2(\theta) + (I_b(\theta)^2 + 2I_a(\theta)I_c(\theta))L_B \sin 2\left(\theta + \frac{2}{3}\pi\right) + (I_c(\theta)^2 + 2I_a(\theta)I_b(\theta))L_B \sin 2\left(\theta + \frac{2}{3}\pi\right) \quad (2-22)$$

The average reluctance torque due to the self-inductance can be expressed by

$$T_{r_{self}} = \frac{1}{\pi} \int_0^\pi I_a(\theta)^2 L_B \sin 2(\theta) + I_b(\theta)^2 L_B \sin 2\left(\theta - \frac{2}{3}\pi\right) + I_c(\theta)^2 L_B \sin 2\left(\theta + \frac{2}{3}\pi\right) d\theta \quad (2-23)$$

Since the IPMSM is a three-phase balanced system, the above average reluctance torque can be simplified as

$$T_{r_{self}} = \frac{3L_B}{\pi} \int_0^\pi I_a(\theta)^2 \sin 2(\theta) d\theta \quad (2-24)$$

Due to the orthogonality of sine function, when $(I_a(\theta))^2$ equals to $\pm P \sin 2(\theta)$, where P determines the magnitude of the sine function, then value of the whole integration is not zero and further simplification can be made to the average torque equation.

Since $\pm \sin 2(\theta)$ can be expressed as $\sin[k+(2-k)]\theta$ and $\sin[k+(-2-k)]\theta$, by selecting the corresponding current harmonics according to the above principle, the equation is simplified as

For $k = 3n, n = 0, \pm 1, \pm 2, \dots$

$$T_{r_{self}} = \frac{2L_B}{\pi} \int_0^\pi I_a(\theta)^2 [\sin 2(\theta) + \sin 2\left(\theta - \frac{2}{3}\pi\right) + \sin 2\left(\theta + \frac{2}{3}\pi\right)] d\theta = 0 \quad (2-25)$$

For $k \neq 3n, n = 0, \pm 1, \pm 2, \dots$

$$\begin{aligned} T_{r_{self}} &= \frac{3L_B}{\pi} \int_0^\pi P \sin 2(\theta)^2 d\theta \\ &= \frac{3L_B}{\pi} \int_0^\pi P \frac{1 - \cos 4(\theta)}{2} d\theta \\ &= \frac{3L_B}{2} P \end{aligned} \quad (2-26)$$

$$T_{r_{mu}} = \begin{cases} 3L_B P & \text{while } k \neq 3n, n = 0, \pm 1, \pm 2, \dots \\ 0 & \text{while } k = 3n, n = 0, \pm 1, \pm 2, \dots \end{cases} \quad (2-27)$$

In which $P = \sum_{-\infty}^{+\infty} [(I_{\alpha k} I_{\beta(2-k)}) - (I_{\alpha k} I_{\beta(-2-k)})]$, the first term is for positive torque production, and the second is for the negative torque production.

The average reluctance torque due to the mutual-inductance can be expressed by

$$\begin{aligned} T_{r_{mu}} &= \frac{1}{\pi} \int_0^\pi 2I_b(\theta)I_c(\theta)L_B \sin 2(\theta) + 2I_a(\theta)I_c(\theta)L_B \sin 2\left(\theta - \frac{2}{3}\pi\right) \\ &\quad + 2I_a(\theta)I_b(\theta)L_B \sin 2\left(\theta + \frac{2}{3}\pi\right) d\theta \end{aligned} \quad (2-28)$$

By applying the same method, further simplification can be given by:

For $k = 3n, n = 0, \pm 1, \pm 2, \dots$

$$T_{r_{mu}} = \frac{2L_B}{\pi} \int_0^\pi I_a(\theta)^2 [\sin 2(\theta) + \sin 2\left(\theta - \frac{2}{3}\pi\right) + \sin 2\left(\theta + \frac{2}{3}\pi\right)] d\theta = 0 \quad (2-29)$$

For $k \neq 3n, n = 0, \pm 1, \pm 2, \dots$

$$\begin{aligned}
T_{r_{self}} &= \frac{6L_B}{\pi} \int_0^\pi P \sin 2(\theta)^2 d\theta \\
&= \frac{6L_B}{\pi} \int_0^\pi P \frac{1 - \cos 4(\theta)}{2} d\theta \\
&= 3L_B P
\end{aligned} \tag{2-30}$$

$$T_{r_{mu}} = \begin{cases} 3L_B P & \text{while } k \neq 3n, n = 0, \pm 1, \pm 2, \dots \\ 0 & \text{while } k = 3n, n = 0, \pm 1, \pm 2, \dots \end{cases} \tag{2-31}$$

In which $P = \sum_{-\infty}^{+\infty} [(I_{\alpha k} I_{\beta(2-k)}) - (I_{\alpha k} I_{\beta(-2-k)})]$, and the total average torque can be given by equation (2-32).

$$T_{avg} = \frac{3}{2} \sum_{-\infty}^{+\infty} \{ (I_{\alpha k} \lambda_k) + 3L_B [(I_{\alpha k} I_{\beta(2-k)}) - (I_{\alpha k} I_{\beta(-2-k)})] \} \tag{2-32}$$

In the above equation, certain combinations of current harmonics can be selected to produce a non-zero average reluctance torque, however, the parts that contribute to the negative torque should be eliminated from the equation if the maximum torque production is desired, secondly, as mentioned from the previous when $k=3n, n=0, \pm 1, \pm 2, \dots$, the average reluctance torque should be zero, so for those current harmonic components that do not contribute to the average torque production, the corresponding current harmonic magnitude should be set to zero, finally, considering in the bandwidth practical drive system and the possibility for real-time implementation, certain restrictions should be set to the current band. Therefore, the following limitations are made:

- The current band is set to be M
- For $k=3n, n=0, \pm 1, \pm 2, \dots, k \in (-M, M), I_{\beta(2-k)}=0$
- For $k \in (-M, M), I_{\beta(2-k)}=0$

By applying all the restrictions, the total average torque is expressed by

$$T_{avg} = \frac{3}{2}p \sum_{-M}^{+M} [(I_{\alpha k} \lambda_k) + 3 L_B (I_{\alpha k} I_{\beta(2-k)})] \quad (2-33)$$

$$\text{For } k = 3n, n = 0, \pm 1, \pm 2, \dots, k \in (-M, M), I_{\beta(2-k)} = 0$$

where p is the number of magnetic pole pairs, L_B equals to $(L_d - L_q)/3$ in $dq0$ frame of references.

2.3 Maximum Torque per Ampere Solution for IPMSM

The MTPA solution can be achieved by using Lagrange optimization method, the MTPA problem is defined as to find the optimal current such that T_{avg} can be maximum, subject to the constant current limit show in (2-34).

$$\frac{3}{2} \sum_{-M}^{+M} (I_{\alpha k}^2 + I_{\beta(2-k)}^2) = C \quad (2-34)$$

Therefore, the Lagrange equation can be defined as

$$\begin{aligned} & f(I_{\alpha k}, I_{\beta(2-k)}, \varepsilon) \\ &= \frac{3}{2} \sum_{-M}^{+M} [(I_{\alpha k} \lambda_k) + 3 L_B (I_{\alpha k} I_{\beta(2-k)})] + \varepsilon \left(\frac{3}{2} \sum_{-M}^{+M} (I_{\alpha k}^2 + I_{\beta(2-k)}^2) - C \right) \end{aligned} \quad (2-35)$$

The optimal current can be obtained by taking the partial derivative of f , the following condition should be met.

$$\frac{\partial f}{\partial I_{\alpha k}} = 0 \quad (2-36)$$

$$\frac{\partial f}{\partial I_{\beta(2-k)}} = 0 \quad (2-37)$$

$$\frac{\partial f}{\partial \varepsilon} = 0 \quad (2-38)$$

For $k = 3n$

$$I_{\alpha k} = \frac{-\lambda_k}{2\varepsilon} \quad (2-39)$$

$$I_{\beta(2-k)} = 0 \quad (2-40)$$

For $k \neq 3n$

$$I_{\alpha k} = \frac{-2\lambda_k \varepsilon}{4\varepsilon^2 - 9L_B^2} \quad (2-41)$$

$$I_{\beta(2-k)} = \frac{3\lambda_k L_B}{4\varepsilon^2 - 9L_B^2} \quad (2-42)$$

And for all the cases,

$$\frac{3}{2} \sum_{-M}^{+M} (I_{\alpha k}^2 + I_{\beta(2-k)}^2) - C = 0 \quad (2-43)$$

As following parameters defined,

$$K_1 = \sum_{-M}^{+M} \lambda_k^2, k \neq 3n \quad (2-44)$$

$$K_2 = \sum_{-M}^{+M} \lambda_k^2, k = 3n \quad (2-45)$$

The solution for ε is given by

$$\varepsilon = -\sqrt{X(p_1, p_2, p_3, p_4)} \quad (2-46)$$

Where $X(p_1, p_2, p_3, p_4)$ is one of the solutions of (2-45)

$$p_1 X^3 + p_2 X^2 + p_3 X + p_4 = 0 \quad (2-47)$$

in which

$$p_1 = \frac{-128C}{3}$$

$$p_2 = 16K_1 + 16K_2 + 192CL_B^2$$

$$p_3 = -72K_1 L_B^2 + 36K_2 L_B^2 - 216CL_B^4$$

$$p_4 = 81K_1L_B^4 \quad (2-48)$$

By solving the equation (2-47) for ε , then the optimal current for MTPA control in IPMSM can be obtained. In practical applications if the BEMF only contains the first order harmonic, $n = 1$ in equation (2-33), then the $I_{\alpha k}$ and $I_{\beta(2-k)}$ are corresponding to I_q and I_d in $dq0$ reference frame, by calculating the value of the two components and equating them to I_q and I_d , real-time implementation can be achieved, if the BEMF exhibits higher order harmonics, certain current harmonic injection methods need to be adopted.

2.4 Summary

The mathematical three-phase model of IPMSM is established, the expression for average torque production and optimal current for MTPA operation is derived through an analytical computation, detailed explanation and discussion have been made.

CHAPTER 3

SIMULATION RESULTS ANALYSIS

3.1 Model Analysis

As mentioned in the previous chapter, the calculation of the optimal current for IPMSM exhibiting non-sinusoidal BEMF requires the information of the flux linkage harmonics created by the permanent magnet. A 1 horsepower IPMSM with three pole pairs was used for simulation. First, the 2D model (shown in Figure 3.1) is built in Ansys Maxwell for finite element analysis (FEA).

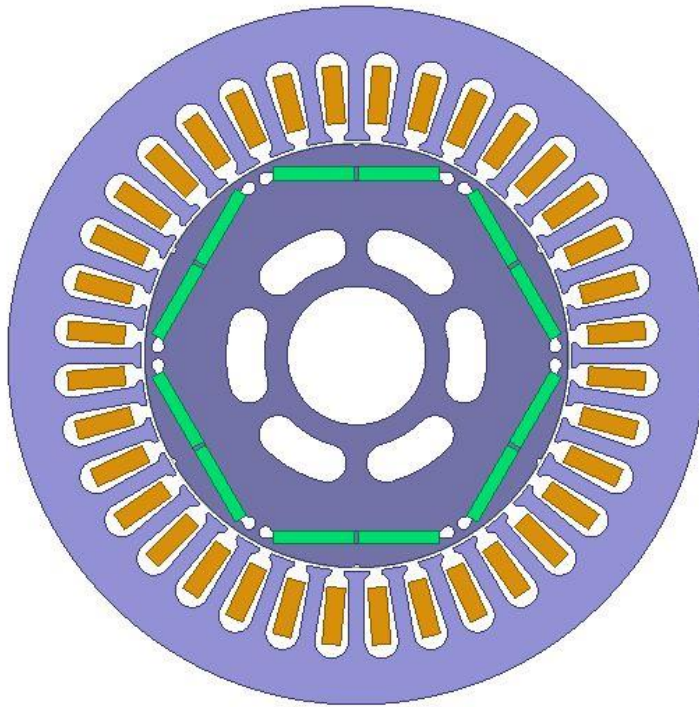


Figure 3.1. 2D model of IPMSM

The mechanical speed of the motor is set to be 200 RPM, and the simulated BEMF is shown in Figure 3.2, and from the same model, flux linkage profile can also be obtained (in Figure 3.3)

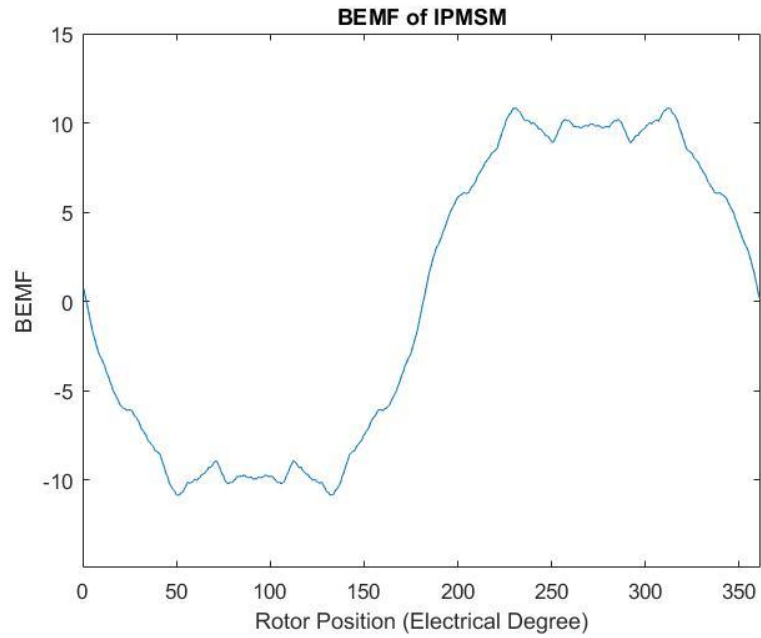


Figure 3.2. BEMF of IPMSM

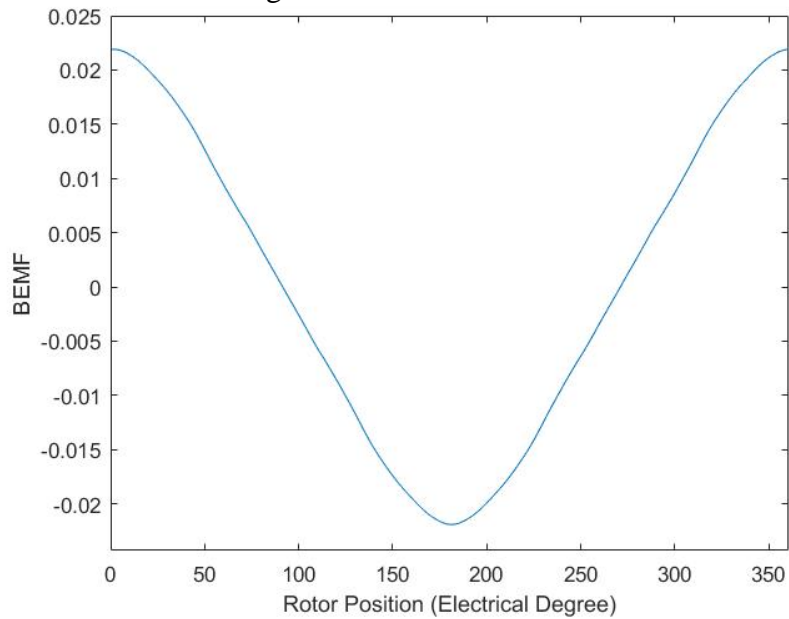


Figure 3.3. Flux Linkage of IPMSM

As clearly shown in Figure 3.2, IPMSM exhibits a non-sinusoidal BEMF, according to the analysis done in Chapter 2, higher order current harmonics should be expected in the expression for optimal current. Hence, firstly, FFT analysis is performed for the flux linkage of IPMSM, the FFT result is shown in Figure 3.4.

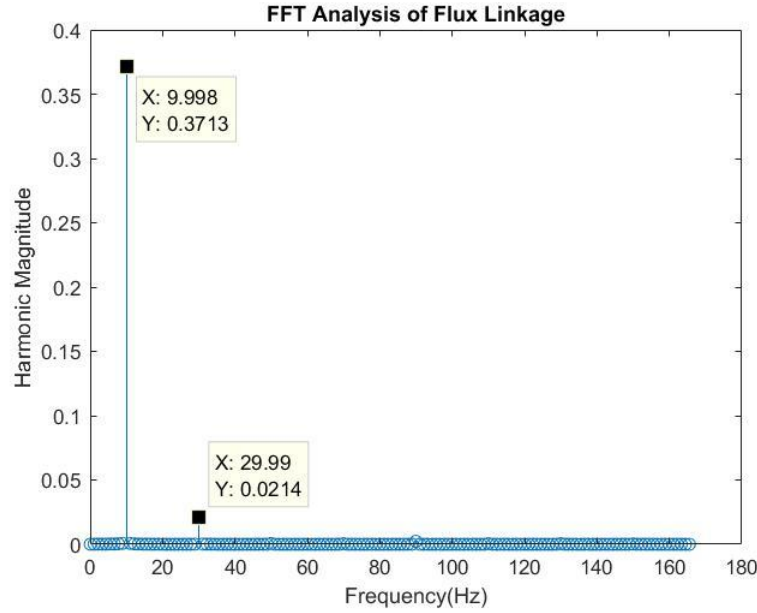


Figure 3.4. FFT Analysis Flux Linkage of IPMSM

From the simulation, the magnitude of each flux linkage harmonic can be obtained, as shown in Figure 3.4, the magnitude of 1st and 3rd flux linkage harmonics are 0.3713 and 0.0214, which can be used to calculate current harmonics for optimal excitation, also, higher order flux linkage harmonics are almost zero, so the band limitation of the motor is set to be 3.

The d-axis and q-axis inductances of the motor are $L_d = 9.9$ mH and $L_q = 21$ mH, as mentioned above, the band limitation of the motor is 3. Therefore, only 1st and 3rd order flux linkage harmonics are taken into consideration and the optimal current in this case should only contain 1st and 3rd current harmonics, calculated values of current harmonics values are listed in Table 1.

Table 1. Magnitude of Current Harmonics (Peak)

Total Current (A)	$I_{\alpha 1}(A)$	$I_{\alpha 3}(A)$	$I_{\beta 1}(A)$
1	0.997	-0.057	-0.0302
1.2	1.197	-0.0689	-0.0435
1.4	1.396	-0.0803	-0.0592
1.6	1.595	-0.0917	-0.0977
1.8	1.794	-0.103	-0.120
2	1.9930	-0.114	-0.120
2.2	2.191	-0.126	-0.145
2.4	2.390	-0.137	-0.173
2.6	2.588	-0.148	-0.202
2.8	2.786	-0.159	-0.234
3.0	2.983	-0.170	-0.268
3.2	3.18	-0.181	-0.305
3.4	3.377	-0.192	-0.343
3.6	3.574	-0.203	-0.384
3.8	3.770	-0.214	-0.427
4.0	3.966	-0.225	-0.472

For 2A peak phase current, Figure 3.5 shows the normalized current waveform of optimal current and sinusoidal current. From the figure, there exists a phase angel between optimal and sinusoidal currents, theoretically, with the increase of the phase current, the angle will finally converge to 45 degrees. The optimal current and sinusoidal current is then injected to the IPMSM model in Maxwell, the torque profiles of both cases can be found in Figure 3.6 and Figure 3.7. From the figure, the optimal current excitation generates a bigger torque than the pure sinusoidal current excitation, the average torque is improved by 0.94%, from numerical calculation, the improvement is 0.714%.

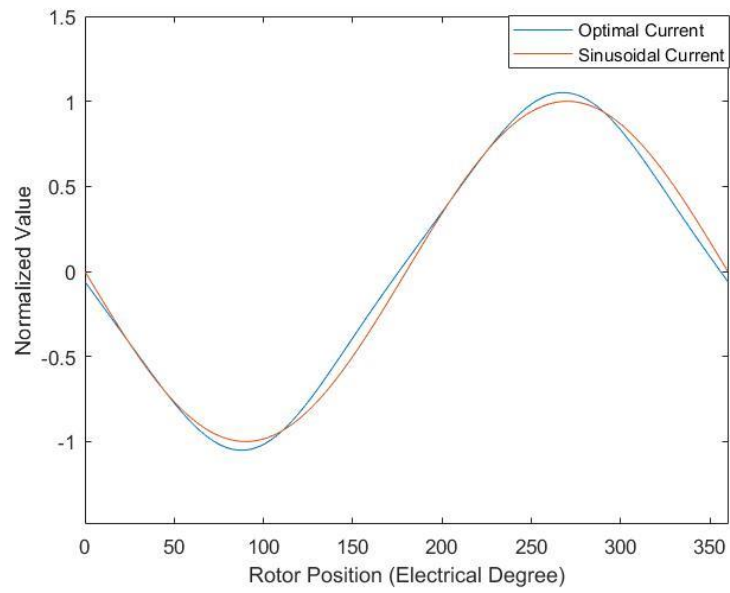


Figure 3.5. Normalized Current Waveform

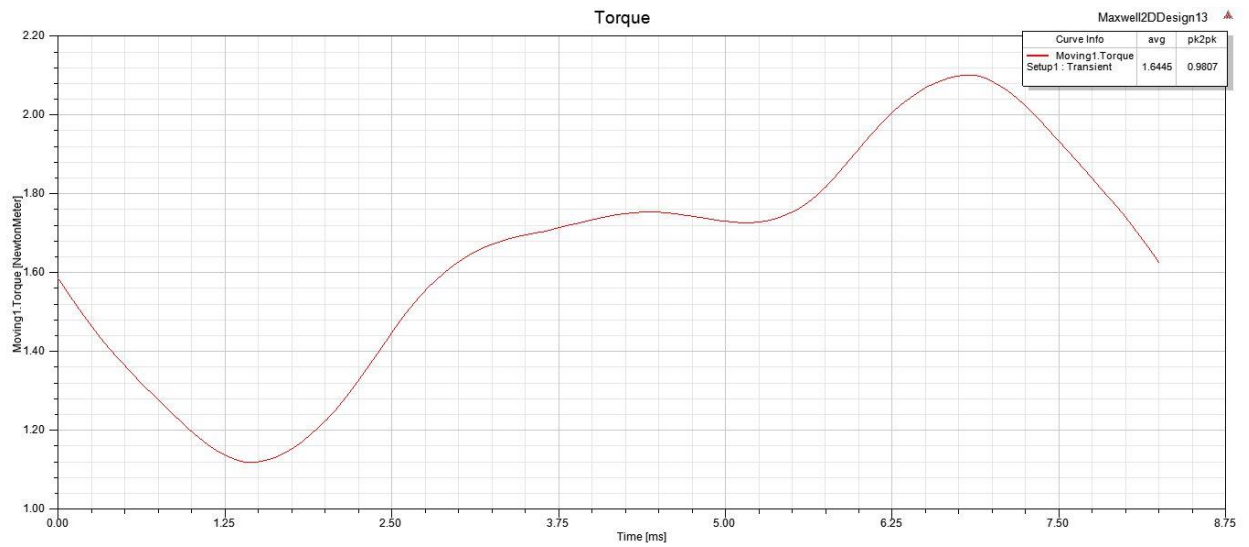


Figure 3.6. Torque Profile of Sinusoidal Current Excitation

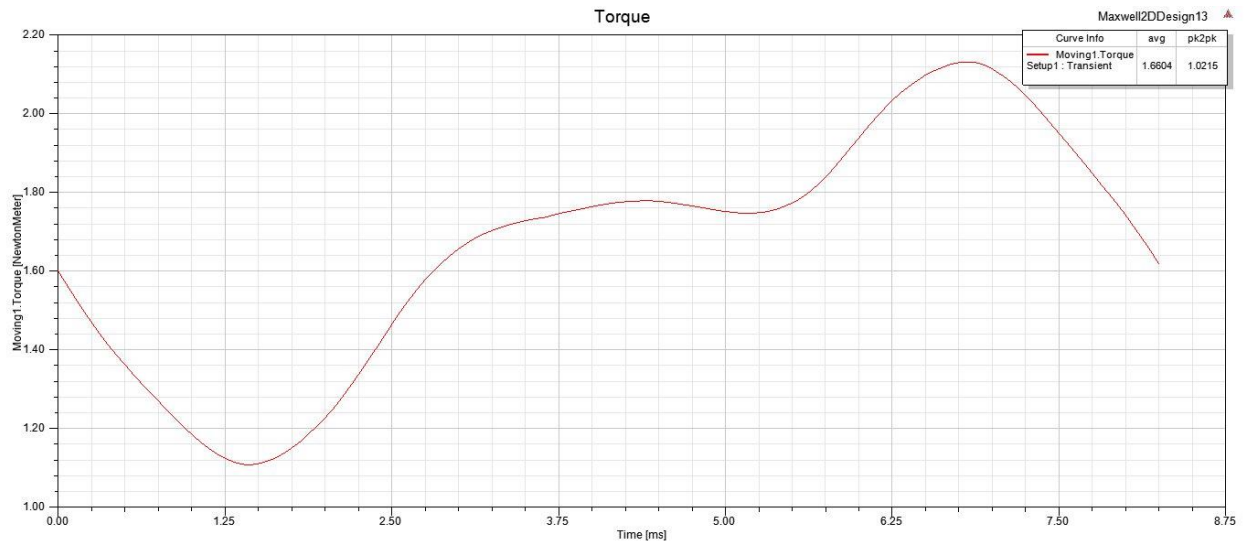


Figure 3.7. Torque Profile of Optimal Current Excitation

The same simulations are done for all the RMS current listed in Table 2, the simulation results and the numerical calculated results are listed in Table 2, Figure 3.8 shows that the simulation results and numerical calculated results.

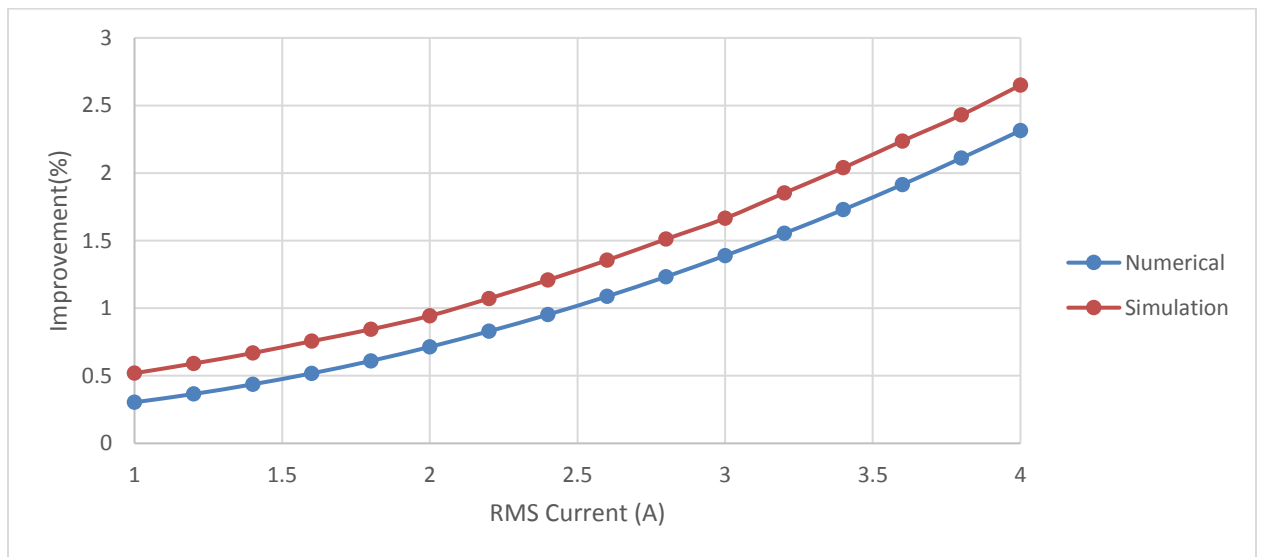


Figure 3.8. Torque Profile of Optimal Current Excitation

Table 2. Simulation and Numerical Calculation Result of Torque Improvement

Total Current (A)	<i>Simulation(%)</i>	<i>Numerical(%)</i>
1	0.519	0.304
1.2	0.604	0.365
1.4	0.668	0.437
1.6	0.749	0.518
1.8	0.843	0.610
2	0.942	0.714
2.2	1.071	0.829
2.4	1.208	0.952
2.6	1.355	1.087
2.8	1.511	1.233
3.0	1.665	1.389
3.2	1.852	1.554
3.4	2.038	1.729
3.6	2.237	1.914
3.8	2.434	2.110
4.0	2.650	2.314

3.2 Current Injection Method

3.2.1 Current Injection Based on FOC

In order to feed the motor with higher order current harmonics, one method is based on adding harmonics in d and q reference frame, in FOC, three-phase alternating currents are decoupled into two-phase currents. If the three-phase alternating currents are pure sinusoidal currents, then the components in d and q reference frame are DC values (shown in Figure 3.9).

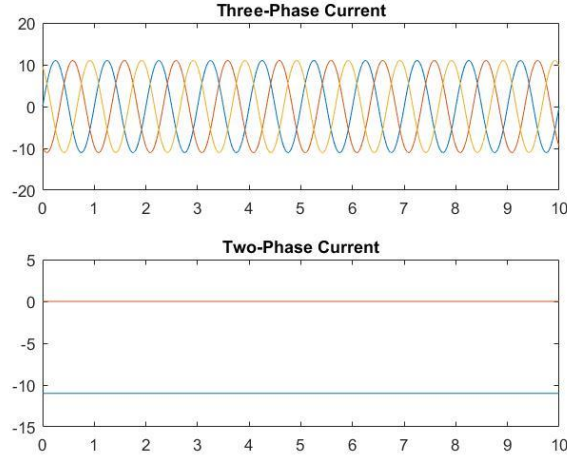


Figure 3.9. Pure Sinusoidal Three-Phase Current and Two-Phase current

If higher order harmonics are required in three-phase current, by adding certain combination of harmonics in d and q reference frame, the goal can be achieved. For example, if the harmonic component of $\sin 3\theta$ is added to d axis and $\cos 3\theta$ is added to q axis, then second order harmonics can be observed in three-phase currents. In the simulation, I_d is set to be 0, I_q is set to -10, and the third order components d and q axis are set to 2. Simulation results are shown in Figure 3.9, and the first subplot is the d and q components. The second subplot is the three-phase current, and the third subplot is the FFT analysis of the current in three-phase frame. The magnitude and frequency of the current harmonics in three phase system are exactly the desired results. For other harmonics, the order of the harmonic and the corresponding sub harmonics in d and q axis are listed in Table 3. Since by implementing FOC, third order current harmonics will be eliminated, so there is no solution in d and q frame if a third order current harmonic is required in three-phase system.

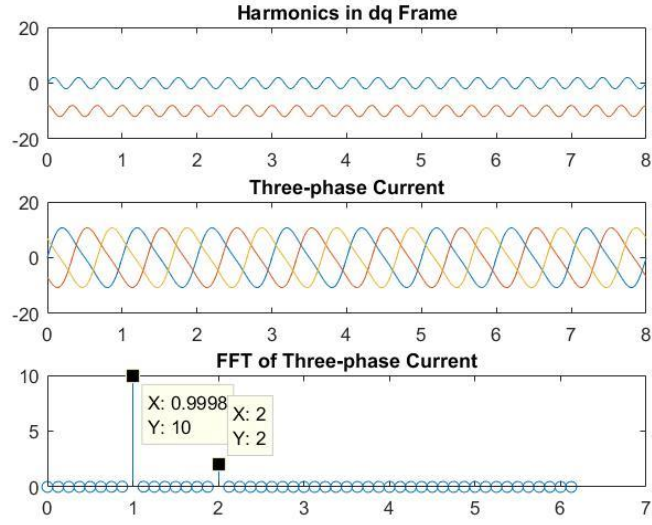


Figure 3.10. Harmonics in dq abc Frame and FFT analysis

Table 3. Relation Between Three-phase and Two-phase Harmonics

Harmonics in three-phase current	Harmonics in d-axis	Harmonics in q-axis
2	$\sin 3\theta$	$\cos 3\theta$
4	$\sin 3\theta$	$-\cos 3\theta$
5	$\sin 6\theta$	$\cos 6\theta$
7	$\sin 6\theta$	$-\cos 6\theta$
8	$\sin 9\theta$	$\cos 9\theta$
10	$\sin 9\theta$	$-\cos 9\theta$
11	$\sin 12\theta$	$\cos 12\theta$
13	$\sin 12\theta$	$-\cos 12\theta$
14	$\sin 15\theta$	$\cos 15\theta$
16	$\sin 15\theta$	$-\cos 15\theta$

In FOC, the control scheme shown in Figure 3.11 is normally used, a Proportional-Integral (PI) regulator is used to control the current in d and q axis, the input of the control system is the current reference, the output of the PI regulator is the desired phase voltage, the output of after the motor

model is the actual current, and then a current feedback is introduced to close the loop for the control system.

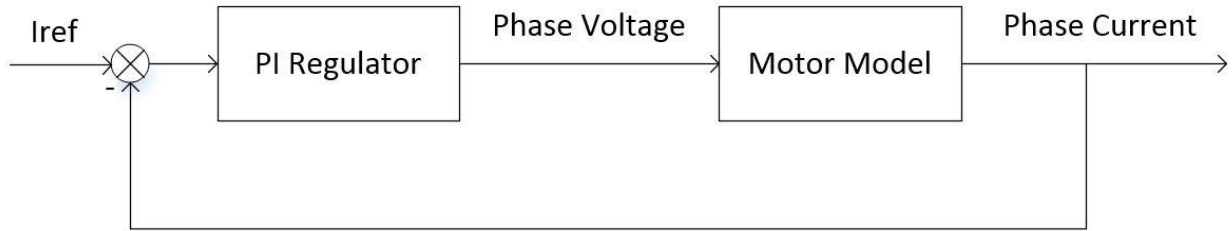


Figure 3.11. Control Scheme of Phase Current

The transfer function of the PI regulator in s-domain is given by

$$PI(s) = \frac{K_p \left(s + \frac{K_i}{K_p} \right)}{s} \quad (3 - 1)$$

According to [26], the motor can model in d and q axis can be represented as

$$V_{qs} = r_s i_{qs} + \frac{dL_q i_{qs}}{dt} + w_e (L_d i_{ds} + \lambda_m) \quad (3 - 2)$$

$$V_{ds} = r_s i_{ds} + \frac{dL_d i_{ds} + \lambda_m}{dt} + w_e L_q i_{qs} \quad (3 - 3)$$

Where V_{qs}, V_{ds} are the phase voltage in d and q axis, i_{ds} and i_{qs} are the current in in d and q axis, λ_m is the flux linkage created by permanent magnet, r_s is the stator resistance, w_e is the rotor electrical angular speed.

And both the current with respect to voltage transfer function in d and can be defined as

$$\frac{I(s)}{U(s)} = \frac{\frac{1}{r_s}}{\frac{L}{r_s} s + 1} \quad (3 - 4)$$

The open loop transfer function in q axis can be defined as

$$T(s) = \frac{\frac{K_p}{r_s} \left(s + \frac{K_i}{K_p} \right)}{s \left(\frac{L_q}{r_s} s + 1 \right)} \quad (3 - 5)$$

By selecting the following parameter, $K_p=1$ and $K_i=500$, the open loop transfer function is given by

$$T(s) = \frac{0.2375s + 118.8}{0.004988s^2 + s} \quad (3 - 6)$$

The bode plot of the open loop transfer function and the step response of the close loop transfer function are given in Figure 3.12 and Figure 3.13, from the bode plot, the phase margin is 74 degrees and the gain margin is infinite, for the step response, the performance is given Table 4.

Table 4. Performance of the step response

Rise Time	0.0153s
Settling Time	0.0221s
Overshoot	1.53%

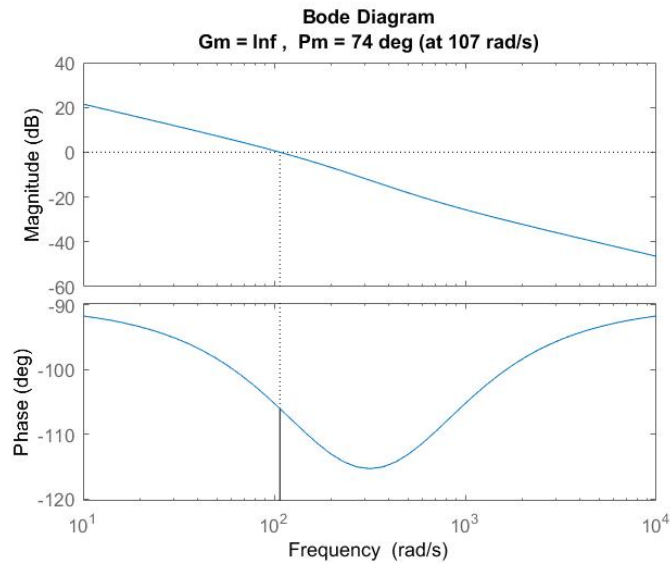


Figure 3.12. Bode Plot of the Open Loop system

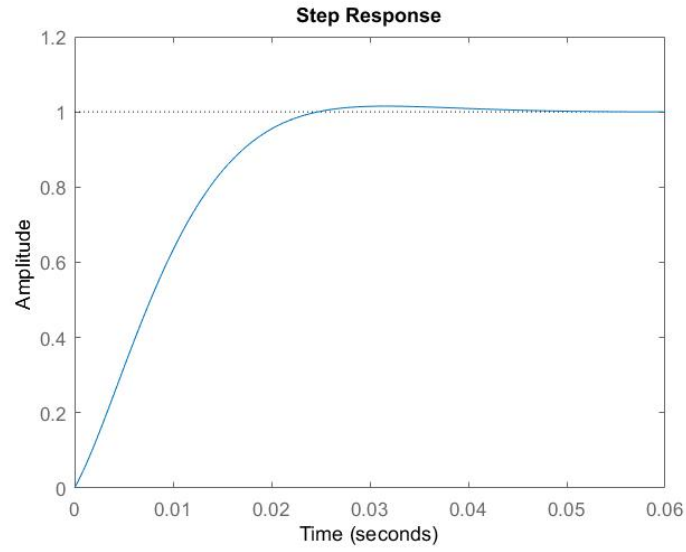


Figure 3.13. Step Response

Since harmonics are introduced in the dq frame, bode plot of the close loop transfer function is also shown in Figure 3.14, as clearly shown in the bode plot, there will be phase shift, so in real time applications, compensation on the rotor angle should be implemented.

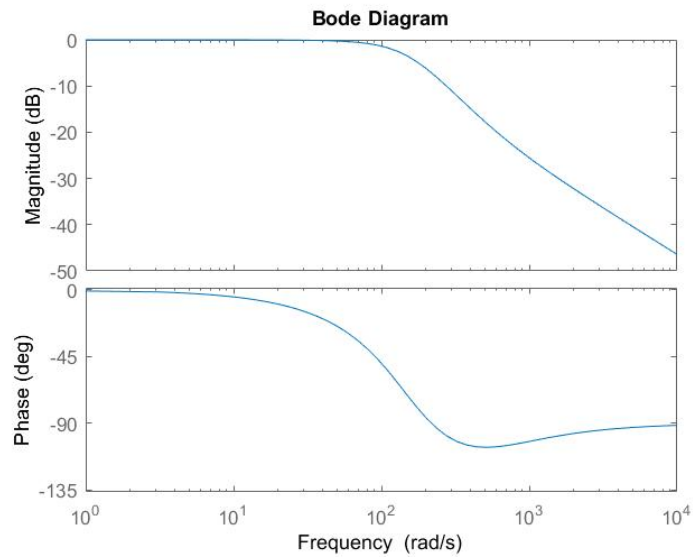


Figure 3.14. Bode Plot of Close Loop System

Simulations were done when the input signal carries the frequency of 10 Hz and 90Hz, and the results are shown in Figure 3.15 and Figure 3.16, significant phase difference and amplitude attenuation can be found if 90 Hz signal is select as the input of the system.

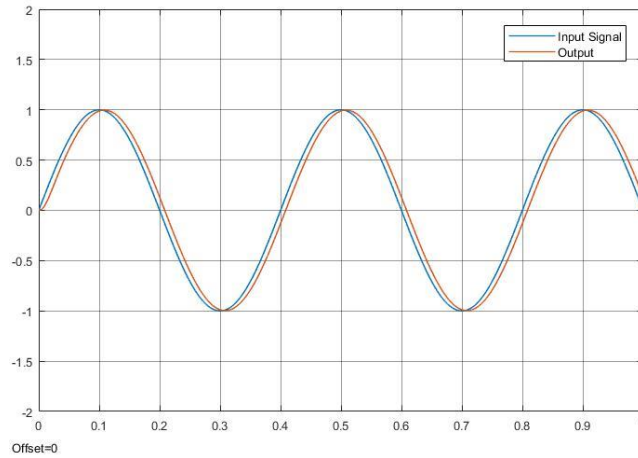


Figure 3.15. Input Signal with Frequency of 10 Hz

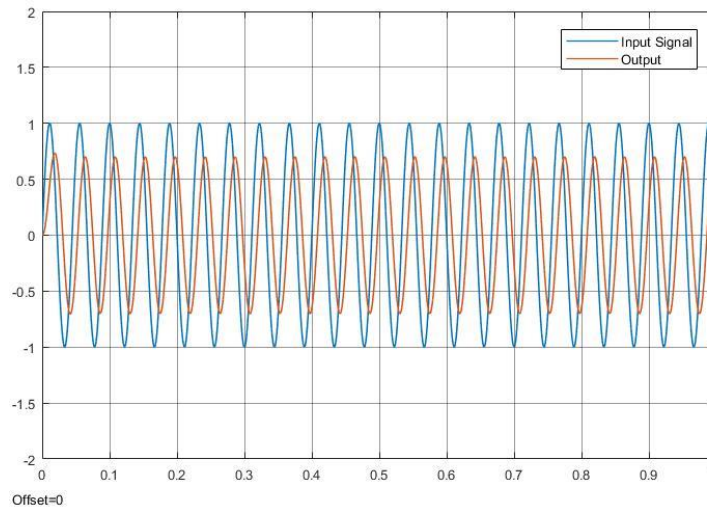


Figure 3.16. Input Signal with Frequency of 90 Hz

Current harmonics injection with FOC might be suitable in low speed applications, since the frequency of the current is relatively low, and there will not be much phase or magnitude difference

between reference and real-time signal, as the frequency increases, certain technique must be implemented to solve the problem, also if the three-phase current requires harmonics whose order is the multiple of 3, this method will not work.

3.2.2 Current Injection Based on Hysteresis Control

Another way of current injection method is based on hysteresis current controller, consider a three-phase inverter connected to a three-phase RL load shown in Figure 3.17, the inverter output current of phase A can be controlled by turning on and off the switching S_1 and S_2 if a reference current i_{ref} is given, there is a current band i_b , then the upper limit is defined as $i_{ref} + i_b$, respectively, the lower limit is defined as $i_{ref} - i_b$.

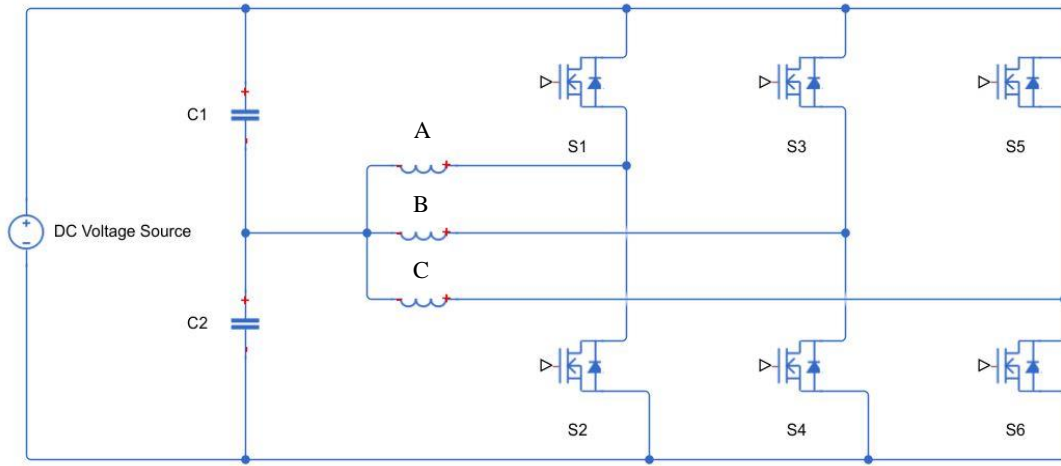


Figure 3.17. Three-phase Inverter Connected to Load

When the actual phase current is between upper and lower limit, there is no switching state change, if the actual phase current is greater than the upper limit, S_1 is turned off, S_2 is turned on, the current starts to decrease, if the current is below the lower limit, then S_2 is turned off, S_1 is turned on, the current increases (shown in Figure 3.18).

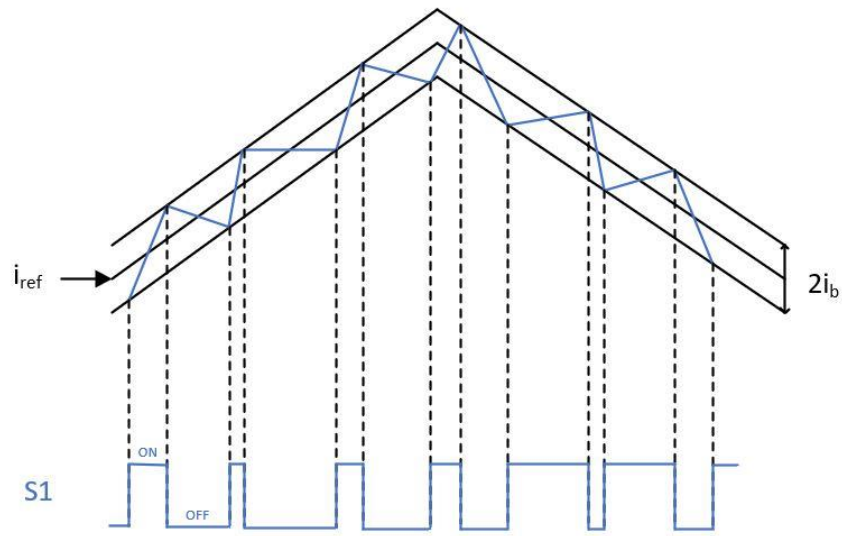


Figure 3.18. Hysteresis Control and Switching Action of S1

The hysteresis current control method is simulated in Matlab/Simulink (shown in Figure 3.19), three phase RL load is connected as Figure 3.14 indicates, and the control logic is shown in Figure 3.20, a script that controls the output current harmonic components is programmed in Reference function block, also, in the hysteresis function block, the current band is selected as 0.1A, and the output is the switching action for the high side switch, and the low side switches have complementary switching actions.

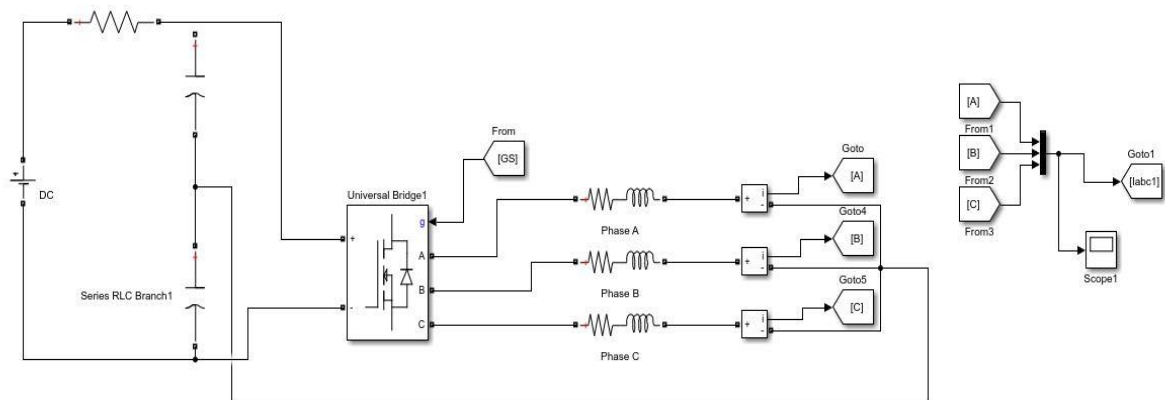


Figure 3.19. Three-phase Inverter with RL Load

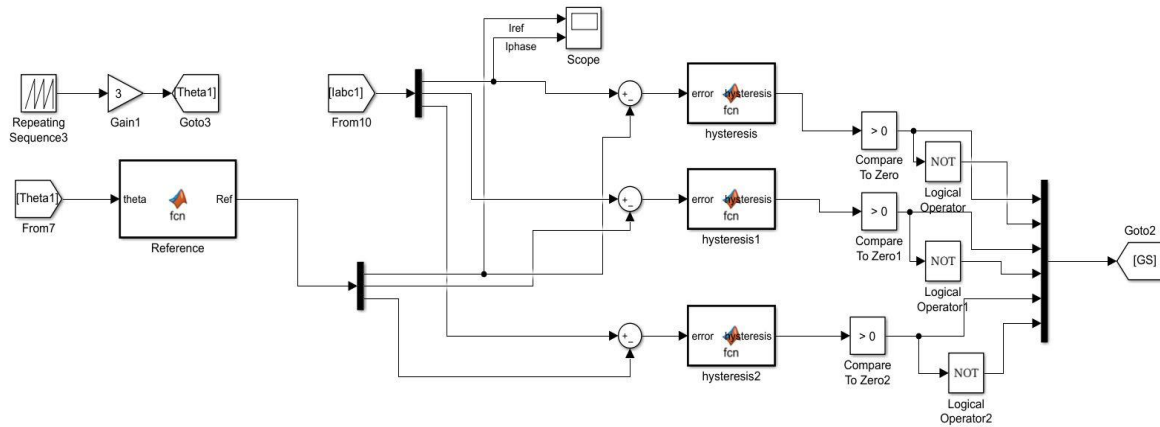


Figure 3.20. Control Logic of Switches

Several simulations are done by setting the reference of current harmonics with different magnitude and frequency. Simulation results together with FFT analysis are shown in 3.21-3.24.

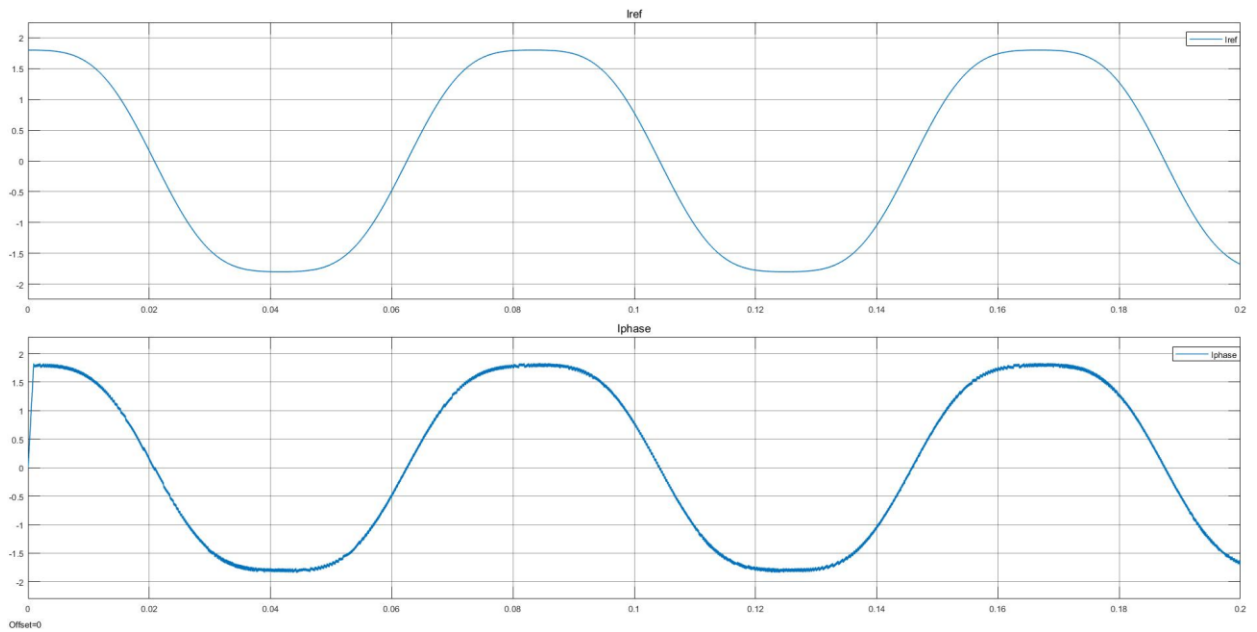


Figure 3.21. First Order Current and Third Order Current

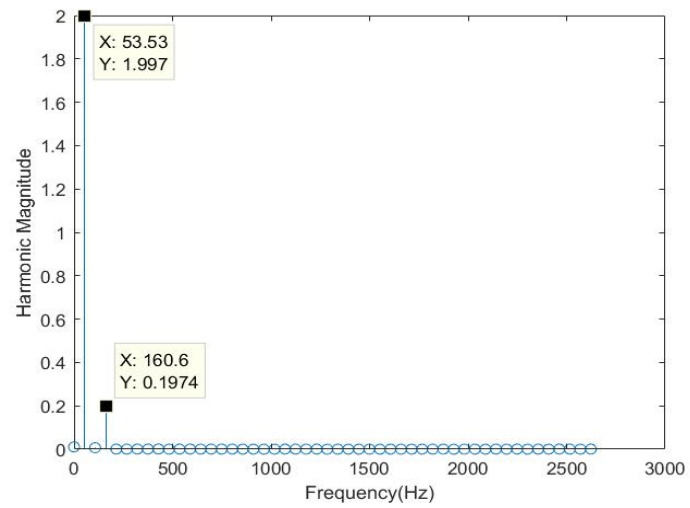


Figure 3.22. FFT Analysis

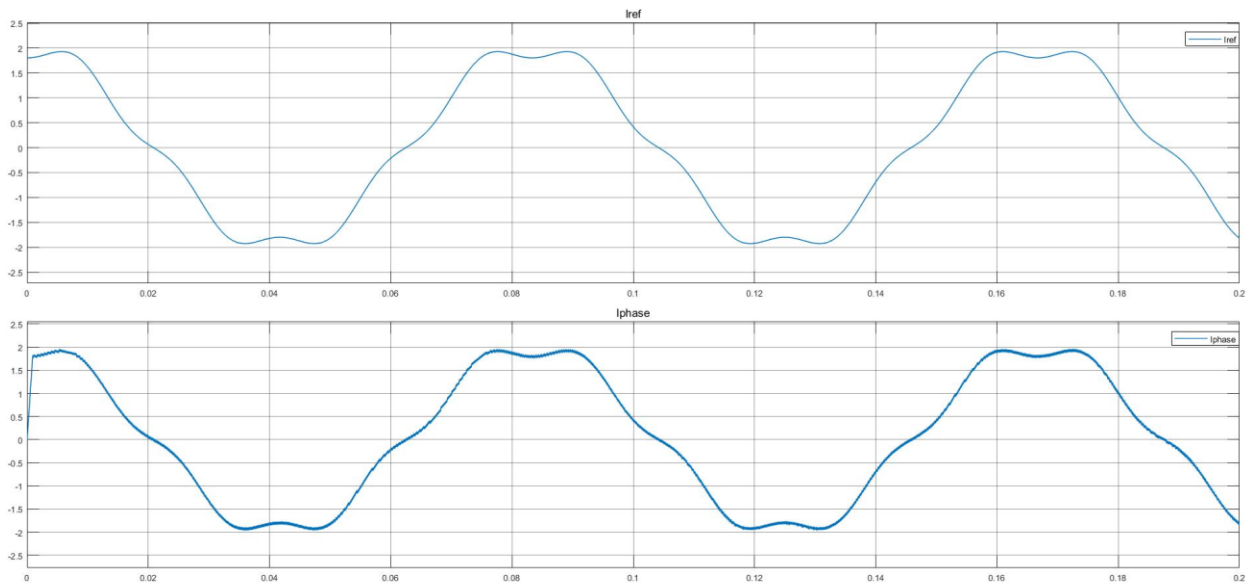


Figure 3.23. First Order Current and Fifth Order Current

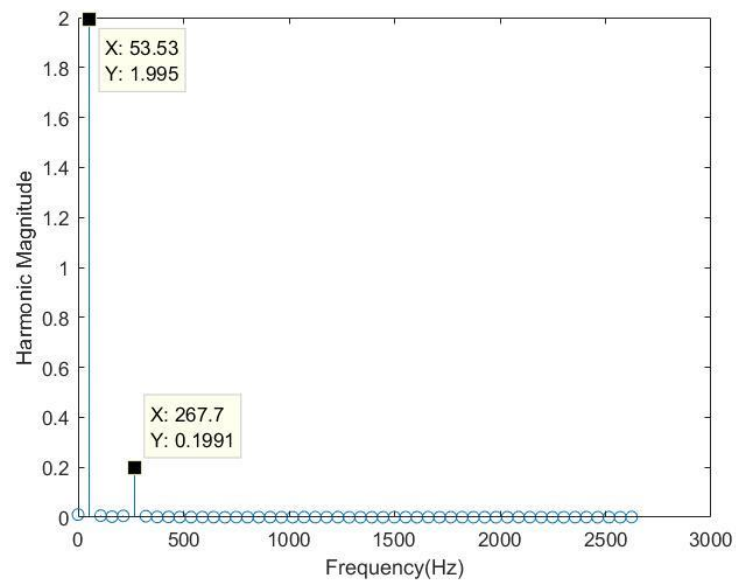


Figure 3.24. FFT Analysis

3.3 Summary

In this chapter, optimal currents have been injected to IPMSM model in FEA, simulation results indicate that the average torque is improved at each RMS current levels. Also, current injection methods have been simulated and a comparison has been made between FOC and hysteresis current control.

CHAPTER 4

EXPERIMENTAL IMPLEMENTATION

4.1 Testbed Introduction

A testbed was built to run the experiments on the test motor, the test platform consists of the following parts, a three-phase inverter was developed to drive the IPMSM, TMS320F28335 is used as the controller for the system, the test motor, the torque meter, DC load motor, a flywheel and the encoder are connected by using couplings, also, the DC load motor is connected to an electrical load that set to the constant voltage mode to provide the whole system with a constant speed since the BEMF of the DC motor cannot exceed the constant voltage set in the electrical load. The testbed is shown in Figure 4.1 with detailed descriptions.

4.2 Hardware Implementation

The scheme of the control system is shown in Figure 4.2, and a printed circuit board (PCB) is designed, shown in Figure 4.3. There are several voltage levels in the PCB that are listed in Table 5.

Table 5. Voltage Levels of Hardware

Inverter Input	120V
Gate Driver	15V
DSP	3.3V

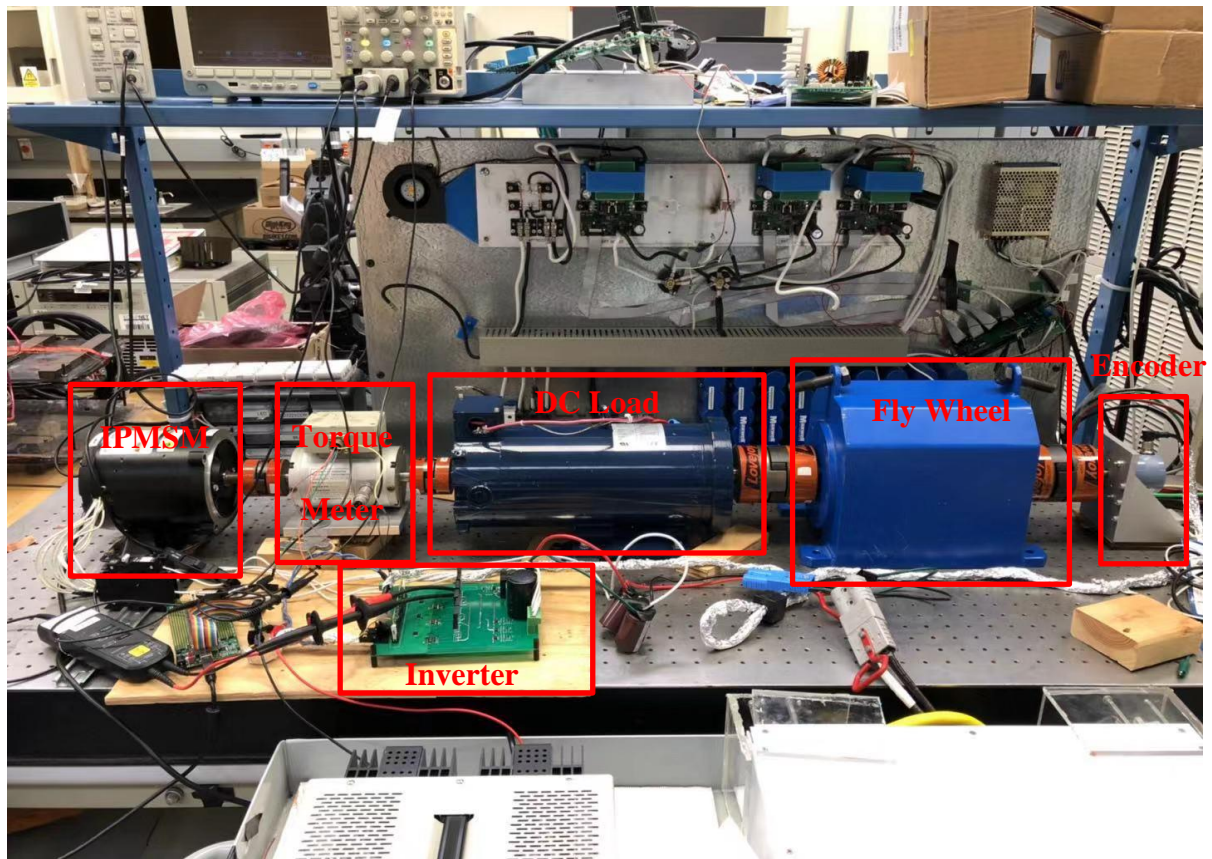


Figure 4.1. IPMSM Control Testbed

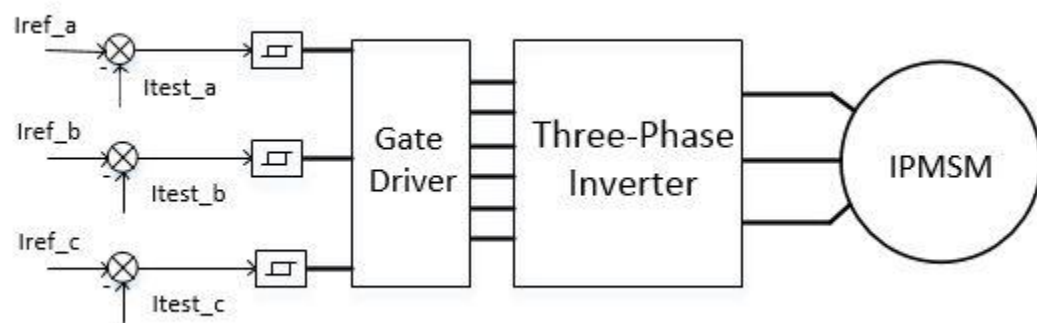
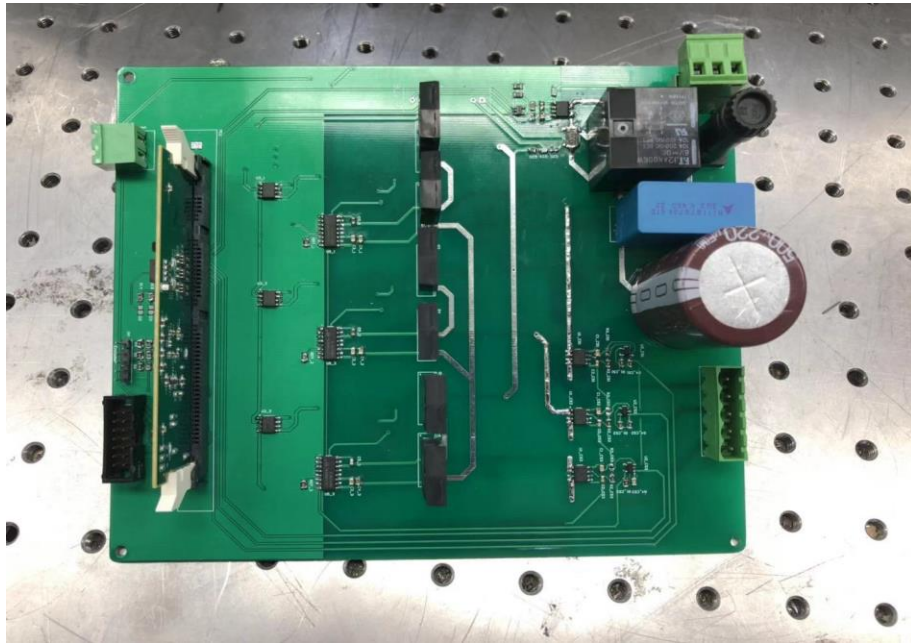
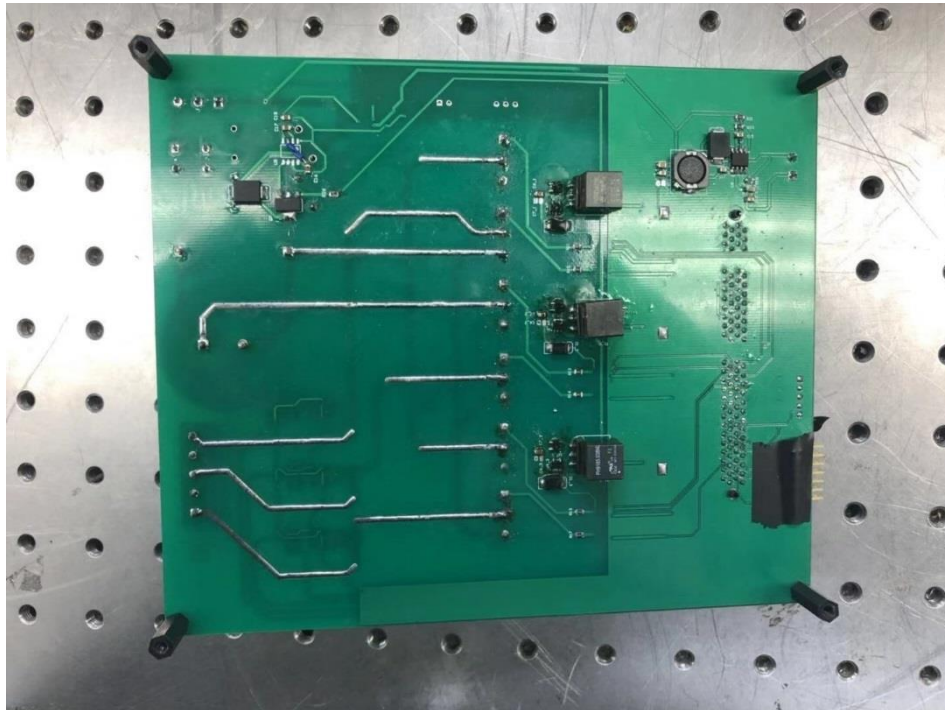


Figure 4.2. Control Scheme of IPMSM



(a)



(b)

Figure 4.3. (a) Top of PCB (b) Bottom of PCB

4.2.1 Design of Gate Driver Power Supply

To turn on a MOSFET, a voltage of 10V to 20V needs to be applied between the gate and source, so an isolated power-supply circuit is made using MAX256 and a transformer (shown in Fig 4.4).

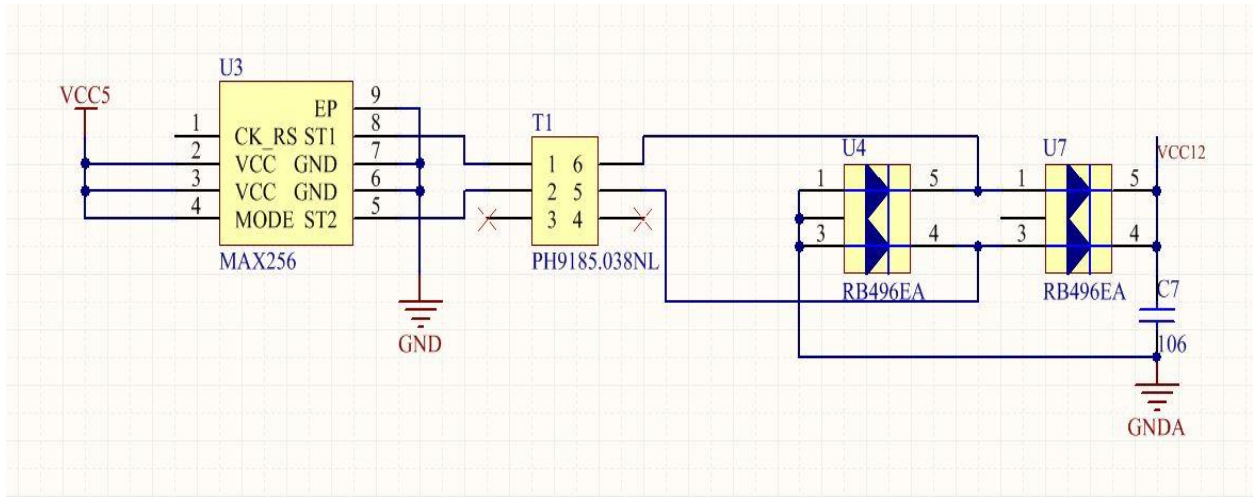


Figure 4.4. Isolated Power Supply Design

MAX256 is powered by an external 5V voltage source, the output of MAX256 are two complementary 50% duty cycle voltage pulses between 0V and 5V, PH9185 is a transformer, in which, the ratio between primary side and secondary side on the PCB is chosen to be 3:10, then, the secondary side voltage pulses pass through a full-bridge rectifier and charge the output capacitor, in this design, the output voltage is around 15V (considering the forward voltage drop of the diode of full bridge rectifier).

Test has been made to verify the design, results are shown in Figure 4.5, the voltage on the primary side, secondary side and the output capacitor are tested in from the PCB, from the figure, we can see that the output voltage is around 15V.

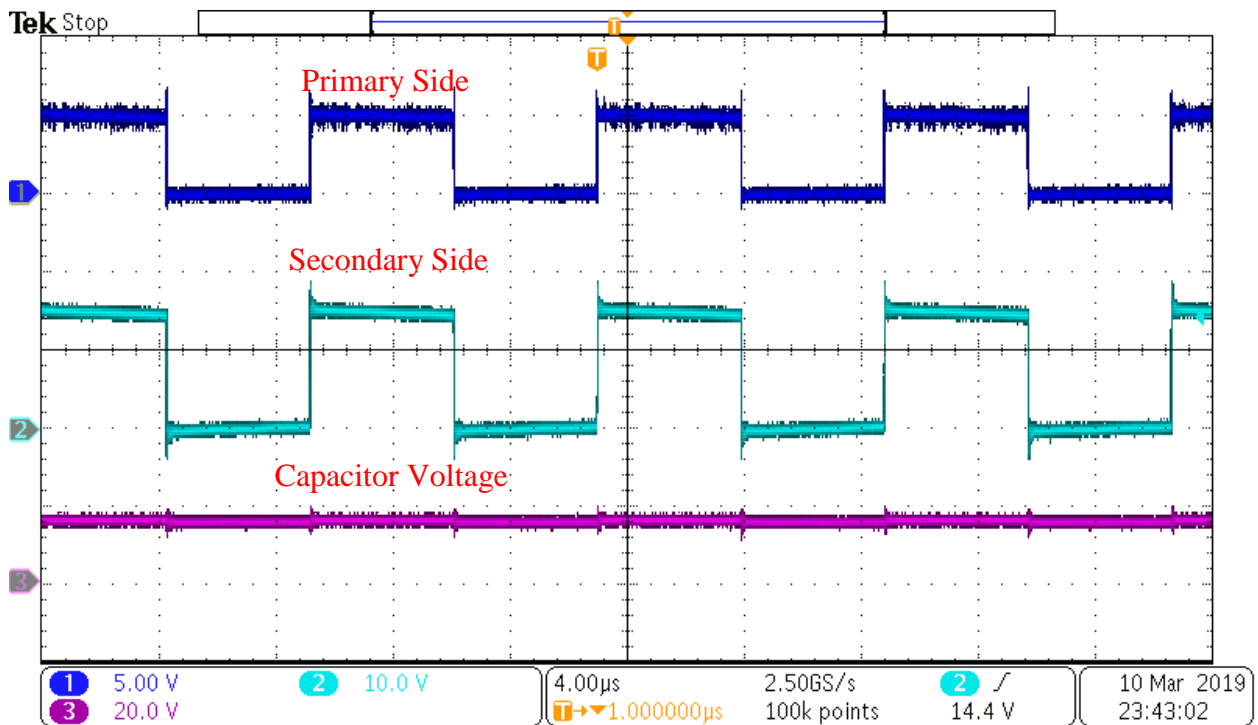


Figure 4.5. Experimental Results of Designed Isolated Power Supply

4.2.2 Design of Gate Driver

In order to control the three-phase inverter, the high side switch also require a 10V to 20V power supply, since the voltage potential of the motor winding is changing while the motor is running, bootstrap circuit is used to drive the high side switch. The schematic of bootstrap circuit is shown in Figure 4.6.

Si8233 is the gate driver, bootstrap diode D1 and bootstrap capacitor C5 consist the bootstrap circuit, in order to successfully turn on the high-side switch, at first, the low-side switch must be turned on to provide a path to charge the high-side bootstrap capacitor. When the high-side switch is off, the power supply tends to charge the capacitor, through the diode, and when the high-side switch is on, the voltage potential on the cathode of the diode is the summation of the voltage on

the motor winding and the bootstrap capacitor, forcing the diode to be reverse biased. PWM_H is the PWM signal for high-side switch, and PWM_L is the PWM signal for low-side switch, DSBL is the disable signal for the gate driver, which can be controlled in the DSP, the value of RDT determines the deadtime insertion period from hardware, G_up is the control signal for high-side switch, and G_down is the control signal for low-side switch, I+ is connected to the motor windings.

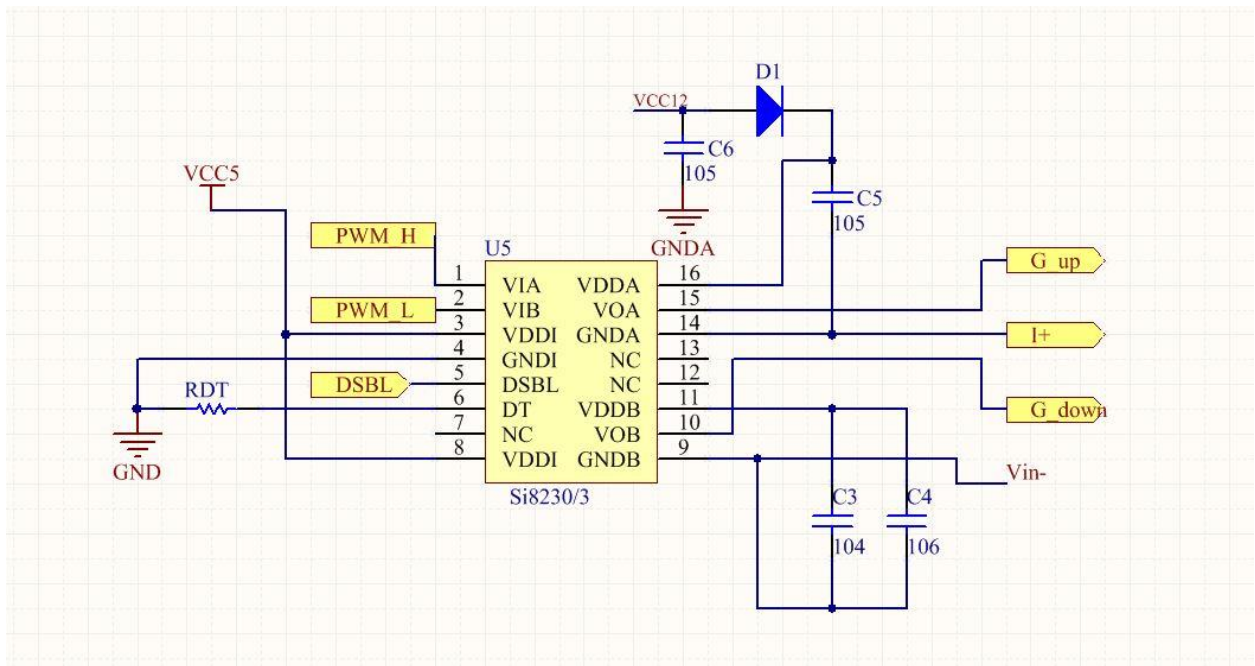


Figure 4.6. Design of Bootstrap Circuit for Three-phase Inverter

Experiment waveform is captured and shown in Figure 4.7. In channel 3, the voltage in the Drain of the high-side switch is captured, and in channel 2 the capacitor voltage is captured. As the high-side switch turns on, the voltage on the capacitor begin to discharge and maintain the on state of the high-side switch. When the high-side switch is off, the power supply begins to charge the capacitor voltage, and a sudden rise in the capacitor voltage can be observed in the figure.

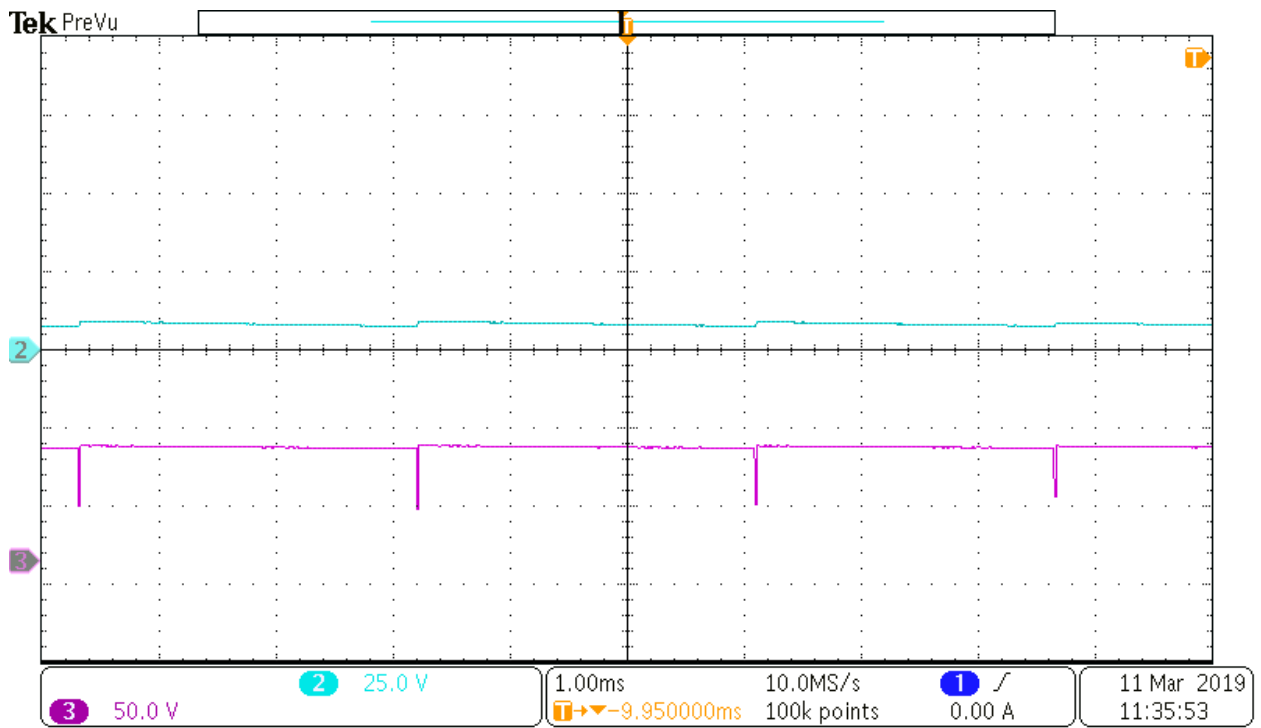


Figure 4.7. Voltage of Bootstrap Capacitor

4.2.3 Design of Current Sensing Circuit

The analog to digital converter (ADC) of the TMS320F28335 has an analog input ranging from 0V to 3V, in the design, the current sensing circuit is shown in Figure 4.8. ACS723-10AB is used to convert the current signal to a output voltage signal, it has an offset of 2.5V, and is capable of sensing both positive and negative current, ranging from -10A to 10A, the output ranges from 0V-5V, so the output cannot be directly connected to the DSP, in the design, a second stage of operational amplifier (op-amp) is designed to tune the output voltage within the input range of ADC by properly choosing the value of R1-R6. The output voltage of the op-amp is given by equation 4-1.

$$V_{out} = V_{sense} * \frac{R_2}{R_3} * \left(\frac{R_4 + R_1}{R_1} \right) - 5 * \left(\frac{R_4 * R_5}{(R_6 + R_5) * R_1} \right) \quad (4 - 1)$$

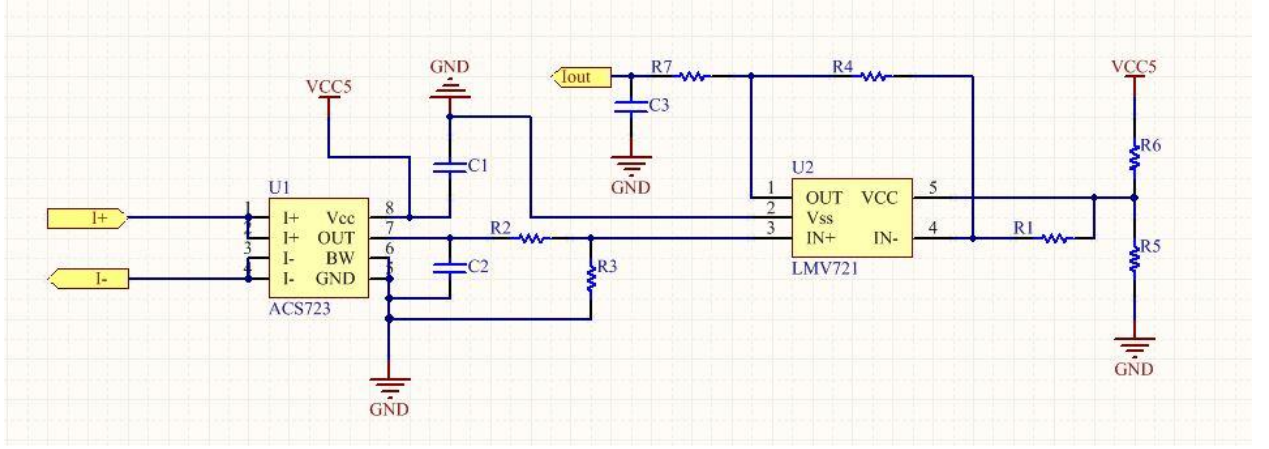


Figure 4.8. Current Sensing Circuit

In the output of the op-amp, there is a RC low pass filter, in which $R=31.8\Omega$, $C=0.1\mu F$ and $f_c=50kHz$. The low-pass filter will clear the high frequency noises in the system. The same low pass filter is implemented on the input signal for encoder interface and the cutoff frequency is designed to be 79kHz.

The experimental implementation details are listed in Table 6.

Table 6. Experimental Implementation Details

Inverter Input	120V
Sampling Rate	20KHz
Deadtime	0.3uS

4.3 Experimental Results

By connecting the DC motor to an electrical load setting at constant voltage mode and connecting a flywheel to the system, the speed of the whole system can be stabilized, the voltage limit of the electrical load is 20V, which maintains the system speed at 200RPM (phase current at 10Hz), by implementing hysteresis control, a sinusoidal current with amplitude of 1A is set as the reference, the experimental results are shown in Figure 4.9.

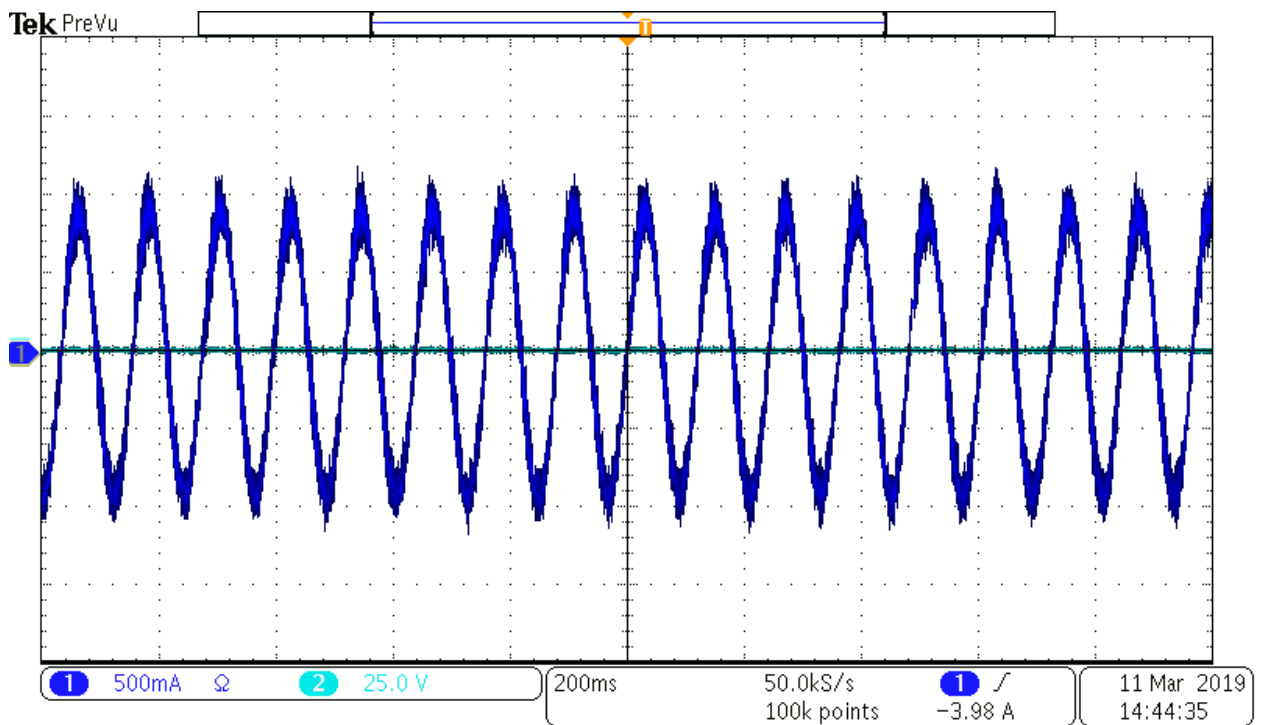


Figure 4.9. Phase Current of 1A

The BEMF of the motor is also measured, by using the dc motor as a prime mover, and the speed is 200RPM, the testing BEMF is shown in Figure 4.10, and comparison between simulation and experiment is shown in Figure 4.11, from the figure, the experimental results matched closely with the simulation.

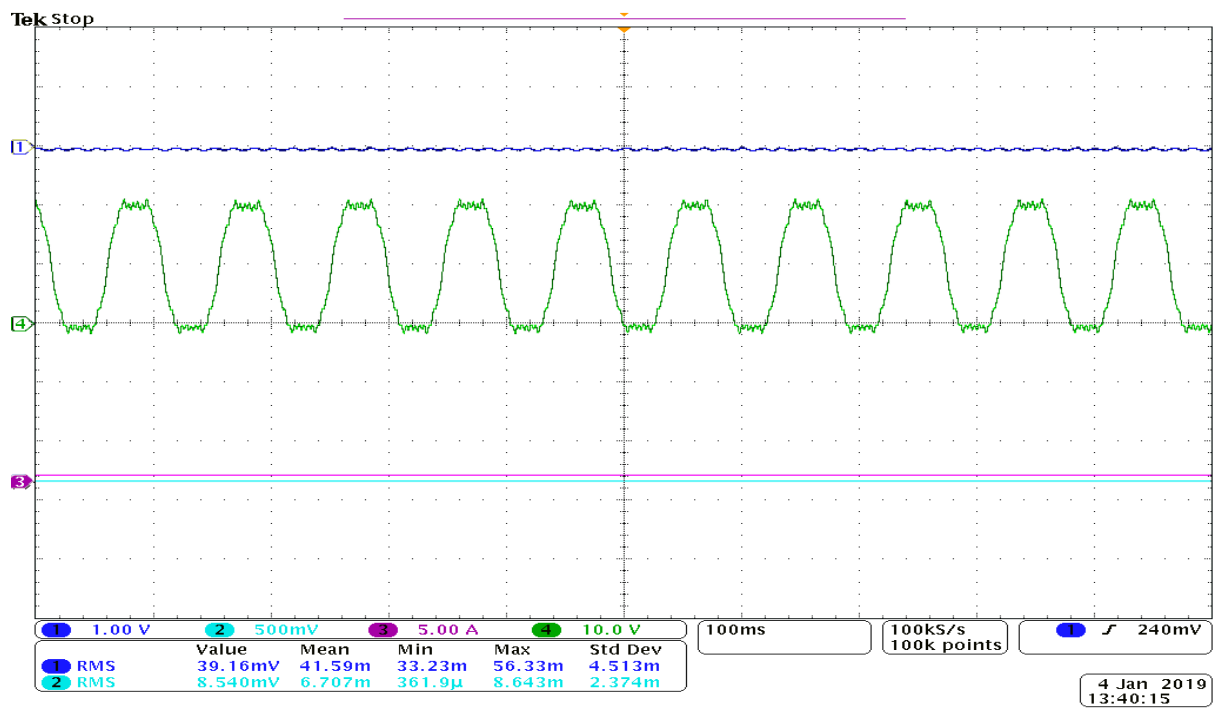


Figure 4.10. Measured BEMF of IPMSM

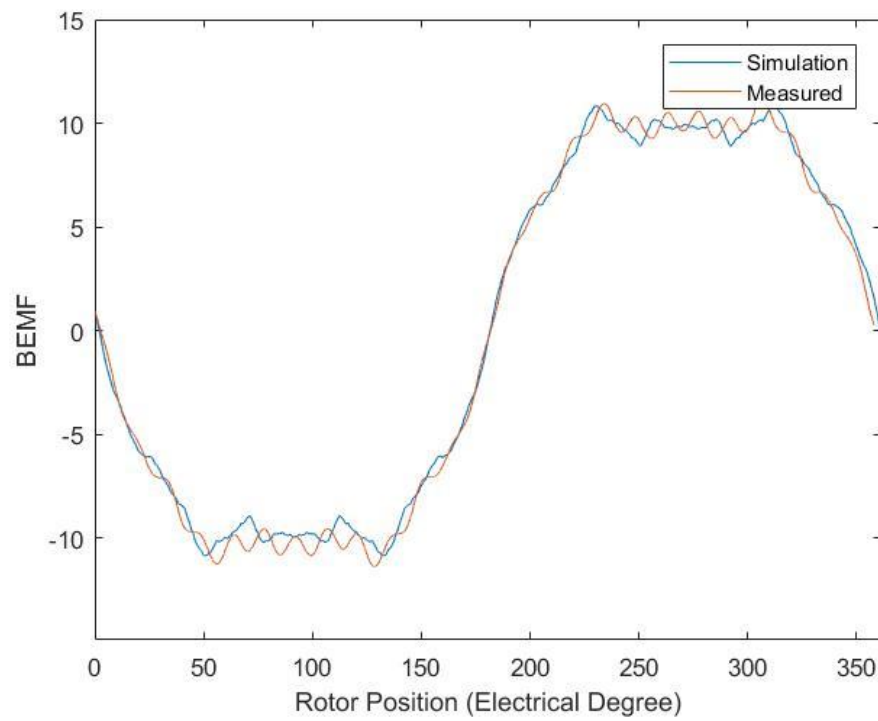


Figure 4.11. Simulated and Measured BEMF

As mentioned above, there are only 1st and 3rd order flux linkage taken into consideration and hence the optimal current should only contain the 1st and 3rd order current harmonics. Calculated values of current harmonics are listed in Table 1. The optimal current was injected into the IPMSM by using hysteresis current control. From the simulation and numerical calculation, the improvement from the tests are less than 1%, so experiments are performed at the peak current level ranging from 2A to 4A. Sinusoidal and optimal current at level of peak 2.2 A and the FFT analysis are shown in Figure 4.12-4.13.

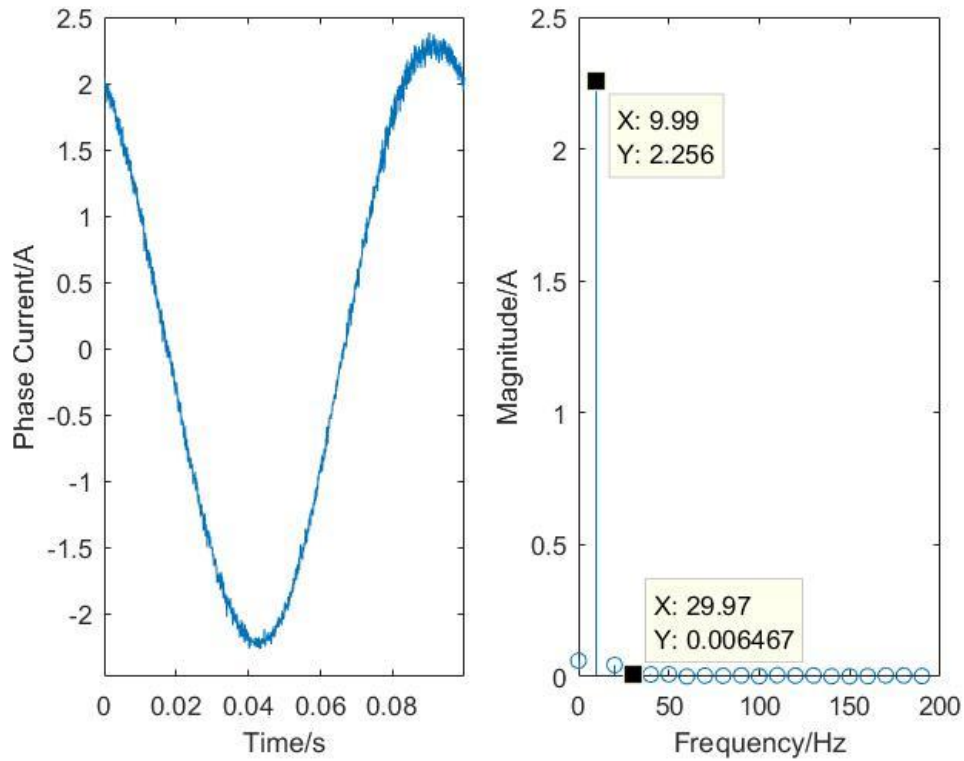


Figure 4.12. Sinusoidal Current at 2.2A Peak

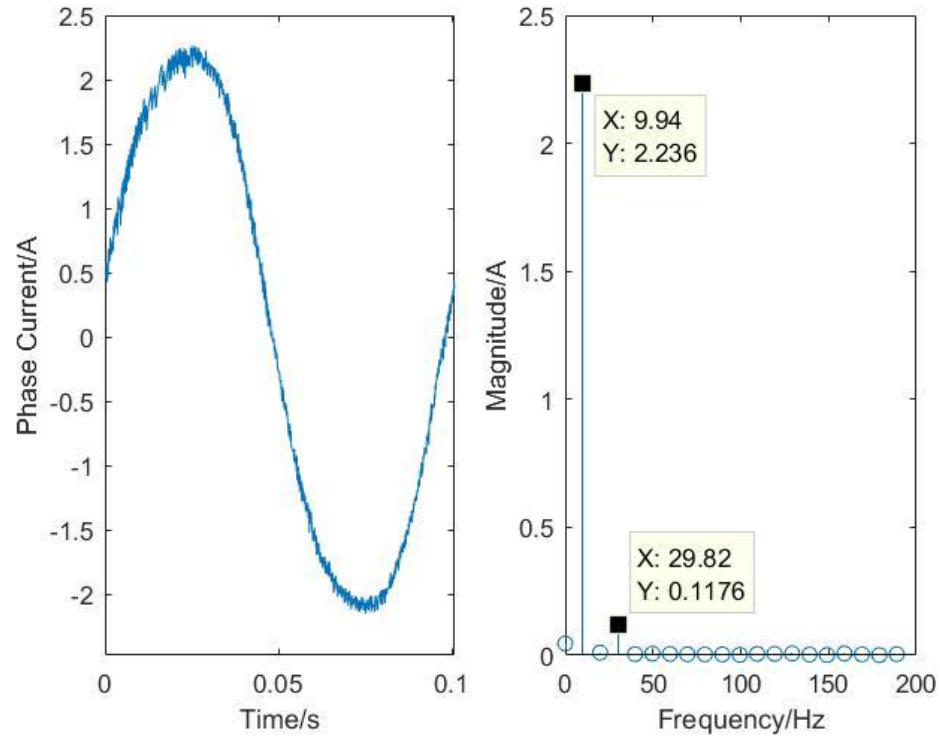


Figure 4.13. Optimal Current at 2.2A Peak

As shown in Figure 4.12 and Figure 4.13, one of the experimental results (total current 2.2A) is presented, from the FFT analysis, the optimal current contains a 1st and 3rd harmonic with magnitude of 2.236A and 0.1176A, which is close to the calculated values (2.191A and 0.126A), Figure 4.14 shows the FFT analysis of the torque, the average torque increased by 1.42% if optimal current is injected, which is close to the simulation result from FEA (1.071%) and numerical calculation (0.829%).

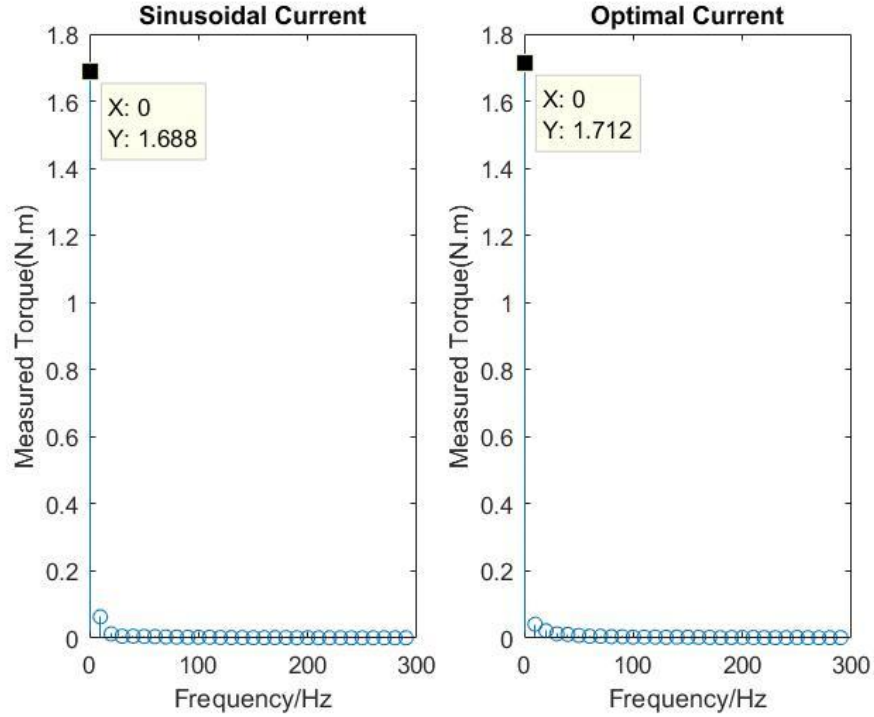


Figure 4.14. Measured Torque and FFT Analysis at 2.2A Peak

Another experiment results at peak 3A is shown in Figure 4.15-4.16, from the results, in optimal current, the measured 1st order current is 3.075A, and the 3rd order current harmonics is 0.1863A, which are close to the calculated value, (1st order of 2.9919A and 3rd order 0.26A), in the sinusoidal current, the amplitude is 3.096A.

In Figure 4.17, the FFT analysis of the torque profile has been done, the average torque increased by 1.39% if optimal current is injected, which is close to the simulation result from FEA (1.84%) and numerical calculation (1.54%). Other test results are listed in Table 7, and a comparison of improvement in torque per ampere (TPA) among experiment, numerical analysis and simulation is shown in Figure 4.18.

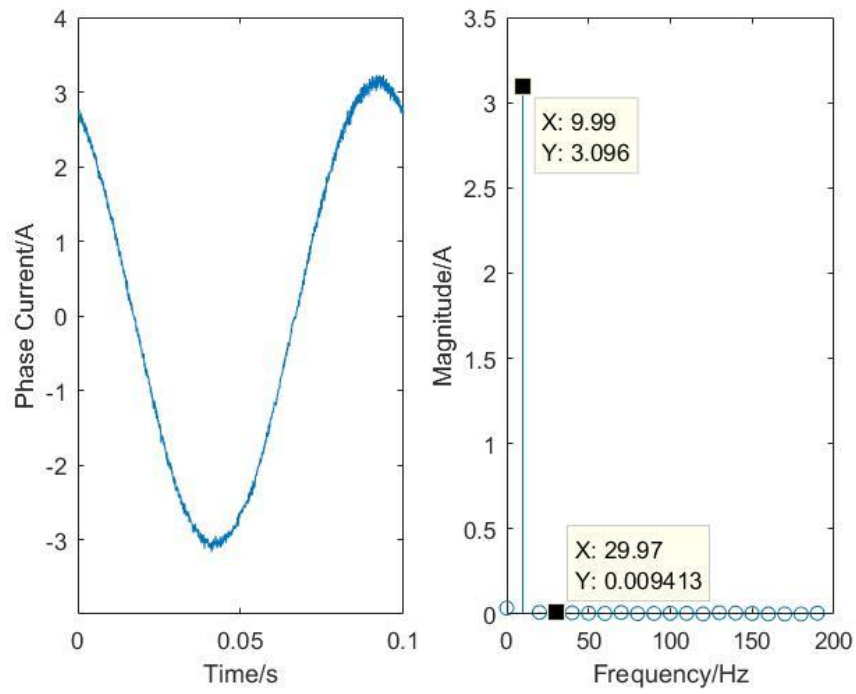


Figure 4.15. Sinusoidal Current at 3A Peak

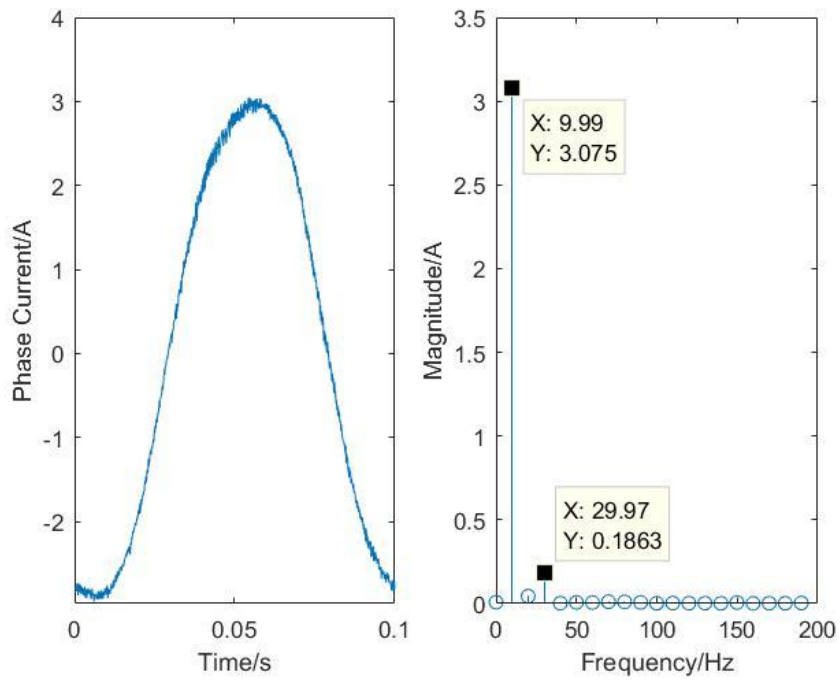


Figure 4.16. Optimal Current at 3A Peak

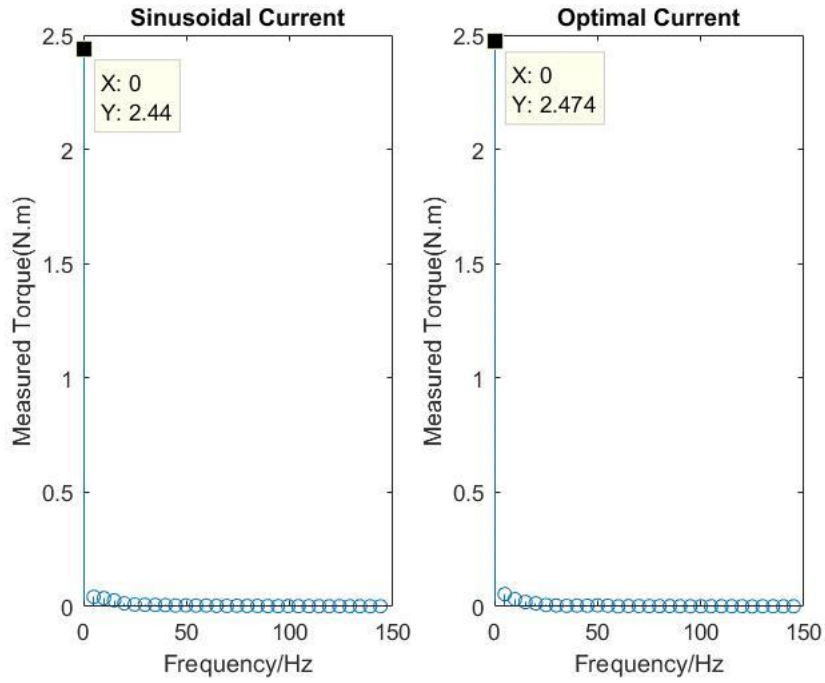


Figure 4.17. Measured Torque and FFT Analysis at 3A Peak

Table 7. Experimental Results Analysis

Peak Current (A)	1 st Order Current (A)	3 rd Order Current (A)	Improvement (%)
2	1.998	0.1042	1.886248
2.2	2.230	0.1176	1.973609
2.4	2.445	0.1169	2.259769
2.6	2.592	0.1376	3.095330
2.8	2.797	0.1308	2.720872
3	3.075	0.1863	1.254634
3.2	3.179	0.1406	1.463793
3.4	3.372	0.2108	3.292969
3.6	3.601	0.1821	2.682374
3.8	3.805	0.2014	3.020273
4	3.994	0.1915	3.265876

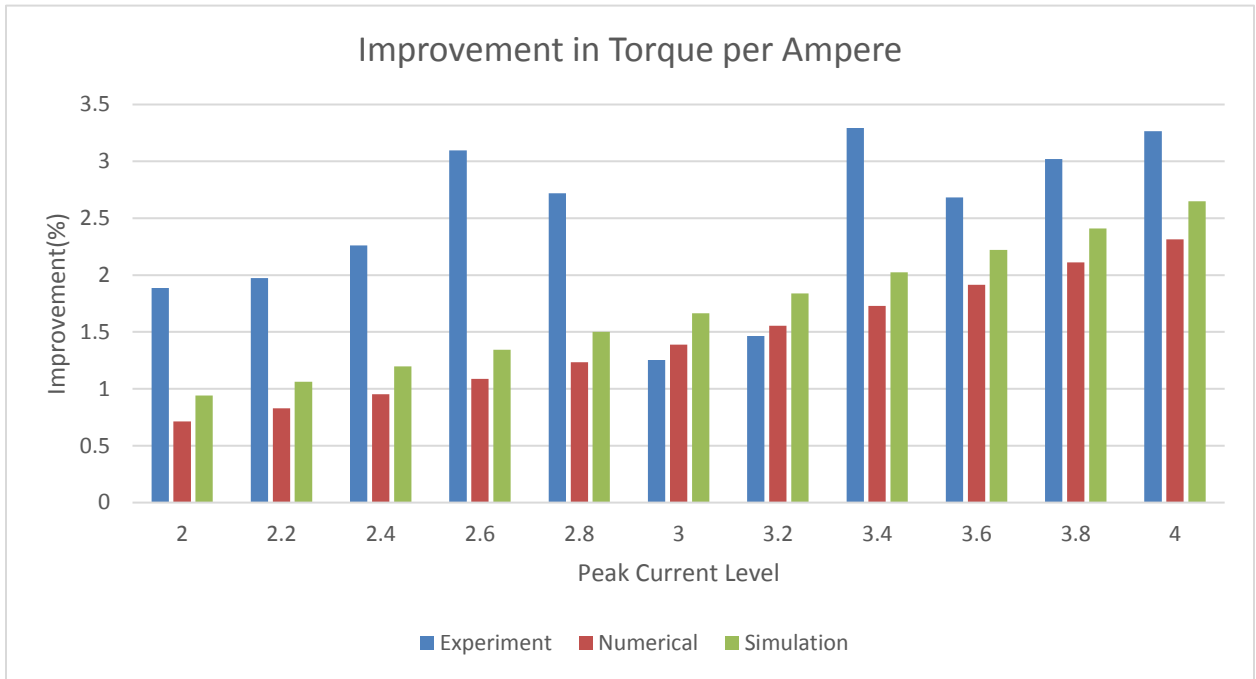


Figure 4.18. Comparison of TPA Improvement

From Figure 4.18, the achieved torque ampere improvements are close to the numerical calculated results and the simulation results (within 2%).

CHAPTER 5

CONCLUSION AND SUGGESTED FUTURE WORK

5.1 Conclusion

In this thesis, an analytical solution for IPMSM MTPA control has been proposed considering IPMSM exhibits harmonics in BEMF, this method can directly calculate the magnitude of all the current harmonics. Then the analytical and simulations in Ansys Maxwell are performed to verify the validity of the proposed method. Due to the third order current harmonic in a phase current, hysteresis current control is used for current injection, hardware and testbed are built for real-time implementation, the experiment also show the satisfactory results.

5.2 Suggested Future work

Although several developments were presented in the thesis, there are many other aspects that needs to be investigated left for future work. Some possible aspects are listed as the following:

- Motor parameters variation needs to be considered
- More experiments should be given on an IPMSM that has a higher rated current or more BEMF harmonics
- A better control approach of current injection method can be explored to solve the problem of varying switching frequency introduced by hysteresis current control

REFERENCES

- [1] C.T. Pan and S.M. Sue, "A linear maximum torque per ampere control for IPMSM drives over full-speed range," *IEEE Transaction Energy Conversion*, vol. 20, no. 2, pp. 359–366,
- [2] P.C. Krause, O. Wasynczuk, S.D. Sudhoff., *Analysis of electric machinery and drive systems*, 2nd ed., John Wiley and sons, New York, 2002. 1995.
- [3] S. Kim, Y. Yoon, S. Sul and K. Ide, "Maximum Torque per Ampere (MTPA) Control of an IPM Machine Based on Signal Injection Considering Inductance Saturation," *IEEE Transactions on Power Electronics*, vol. 28, no. 1, pp. 488-497, Jan. 2013.
- [4] S. Morimoto, K. Hatanaka, Y. Tong, Y. Takeda and T. Hirasu, "High performance servo drive system of salient pole permanent magnet synchronous motor," *Conference Record the 1991 IEEE Industry Applications Society Annual Meeting*, Dearborn, MI, 1991, pp. 463-468 vol.1.
- [5] S. Morimoto, Y. Takeda, T. Hirasu and K. Taniguchi, "Expansion of operating limits for permanent magnet motor by current vector control considering inverter capacity," *IEEE Transactions on Industry Applications*, vol. 26, no. 5, pp. 866-871, Sept.-Oct. 1990.
- [6] T. M. Jahns, G. B. Kliman and T. W. Neumann, "Interior Permanent-Magnet Synchronous Motors for Adjustable-Speed Drives," *IEEE Transactions on Industry Applications*, vol. IA-22, no. 4, pp. 738-747, July 1986.
- [7] T. Sebastian, "Temperature effects on torque production and efficiency of PM motors using NdFeB magnets," *IEEE Transactions on Industry Applications*, vol. 31, no. 2, pp. 353-357, March-April 1995.
- [8] Y. A. -. I. Mohamed and T. K. Lee, "Adaptive self-tuning MTPA vector controller for IPMSM drive system," *IEEE Transactions on Energy Conversion*, vol. 21, no. 3, pp. 636-644, Sept. 2006.
- [9] N. Bedetti, S. Calligaro and R. Petrella, "Self-adaptation of MTPA tracking controller for IPMSM and SynRM drives based on on-line estimation of loop gain," *2017 IEEE Energy Conversion Congress and Exposition (ECCE) Cincinnati, OH*, 2017, pp. 1917-1924.
- [10] P. Niazi, H. A. Toliyat and A. Goodarzi, "Robust Maximum Torque per Ampere (MTPA) Control of PM-Assisted SynRM for Traction Applications," *IEEE Transactions on Vehicular Technology*, vol. 56, no. 4, pp. 1538-1545, July 2007.

- [11] Q. Liu and K. Hameyer, "High-Performance Adaptive Torque Control for an IPMSM With Real-Time MTPA Operation," *IEEE Transactions on Energy Conversion*, vol. 32, no. 2, pp. 57
- [12] P.C. Krause, O. Wasynczuk, S.D. Sudhoff., *Analysis of electric machinery and drive systems*, 2nd ed., John Wiley and sons, New York, 2002. 1995.
- [13] T.M. Jahns, "Toque Production in Permanent-Magnet Synchronous Motor Drives with Rectangular Current Excitation," in *IEEE Transaction on Industry Applications*, VocIA-20, No. 4, 1984, pp. 803-813.
- [14] P. L. Chapman, S. D. Sudhoff and C. A. Whitcomb, "Optimal current control strategies for surface-mounted permanent-magnet synchronous machine drives," *IEEE Transaction on Energy Conversion*, vol. 14, no. 4, pp. 1043-1050, Dec. 1999.
- [15] A. P. Wu and P. L. Chapman, "Simple expressions for optimal current waveforms for permanent-magnet synchronous machine drives," *IEEE Transactions on Energy Conversion*, vol. 20, no. 1, pp. 151-157, March 2005.
- [16] P. L. Chapman and S. D. Sudhoff, "A multiple reference frame synchronous estimator/regulator," *IEEE Transactions on Energy Conversion*, vol. 15, no. 2, pp. 197-202, June 2000.
- [17] J. Wang, Z. Li, L. Xu and L. Zhou, "Novel vector control technique for IPM brushless machines with non-sinusoidal back-EMF," 2016 19th International Conference on Electrical Machines and Systems (ICEMS), China, 2016, pp. 1-6.
- [18] J. Wang, L. Xu, Z. Li, X. Liu and L. Zhou, "An optimal current reference generation Method for IPM brushless machines with non-sinusoidal back-EMF," 2016 IEEE 8th International Power Electronics and Motion Control Conference (IPEMC- ECCE Asia), Hefei, 2016, pp. 846-850.
- [19] S. Park, H. Park, M. Lee and F. Harashima, "A new approach for minimum-torque-ripple maximum-efficiency control of BLDC motor," *IEEE Transactions on Industrial Electronics* vol. 47, no. 1, pp. 109-114, Feb. 2000.
- [20] W. Wang, B. Fahimi and M. Kiani, "Maximum torque per ampere control of Permanent Magnet Synchronous Machines," 2012 XXth International Conference on Electrical Machines, Marseille, 2012, pp. 1013-1020.
- [21] G. Buja, M. Bertoluzzo and R. K. Keshri, "Torque Ripple-Free Operation of PM BLDC Drives With Petal-Wave Current Supply," *IEEE Transactions on Industrial Electronics* vol. 62, no. 7, pp. 4034-4043, July 2015.

- [22] M. Kadjoudj, M. E. H. Benbouzid, C. Ghennai and D. Diallo, "A robust hybrid current control of permanent-magnet synchronous motor drive," *IEEE Transactions on Energy Conversion*, vol. 19, no. 1, pp. 109-115, March 2004.
- [23] F. Caricchi, F. Crescimbeni, T. A. Lipo and E. Santini, "Innovative inverter topology for concentrated winding PM motor drives," *PESC '92 Record. 23rd Annual IEEE Power Electronics Specialists Conference*, Toledo, Spain, 1992, pp. 964-972 vol.2.
- [24] W. Zhang, S. Huang, J. Gao, R. Li and L. Dai, "Electromagnetic Torque Analysis for All-Harmonic-Torque Permanent Magnet Synchronous Motor," *IEEE Transactions on Magnetics*, vol. 54, no. 11, pp. 1-5, Nov. 2018, Art no. 8206405.
- [25] J. Fang, C. Heising, V. Staudt and A. Steimel, "Modelling of anisotropic synchronous machine in stator-reference frame including torque calculation," *Electrical Systems for Aircraft, Railway and Ship Propulsion, Magnetics*, Bologna, 2010, pp. 1-6. doi: 10.1109/ESARS.2010.5665225
- [26] S. Carpiuc, D. Patrascu and C. Lazar, "Optimal torque control of the Interior Permanent Magnet Synchronous Machine," *2011 XXIII International Symposium on Information, Communication and Automation Technologies*, Sarajevo, 2011, pp. 1-8.

BIOGRAPHICAL SKETCH

Taowen Chen was born in Huzhou, China. He received his Bachelor of Engineering (BE) in Electrical Engineering from Nanjing Institute of Technology, Nanjing, China in 2017. He was admitted to the program of Electrical Engineering in Fall 2017 at The University of Texas at Dallas. He joined the Renewable Energy and Vehicular Technology Laboratory (REVT) as a student worker. His research interests include power electronics and motor control.

CURRICULUM VITAE

Taowen Chen

University of Texas at Dallas, Richardson, TX

Master of Science, Electrical Engineering (Power Electronics)

May 2019

Nanjing Institute of Technology, School of Automation, China

Bachelor of Science, Electrical Engineering

June 2017

SKILLS

Technical Software Packages: Matlab/Simulink, CCS, Keil MDK, Altium Design, ANSYS, LTSpice

Programming Languages: Python, C, Micro-Controller programming TI F28335, MSP430, STM32F1

WORK EXPERIENCE

Renewable Energy and Vehicular Technology Lab, University of Texas at Dallas (May 2018 – May 2019)

Graduate Student Worker

- **DC-DC Buck Converter Design** **Mar 2019 – Present**
 - Design schematics and PCB layout
 - Average model analysis of Buck converter and PI controller design
 - Simulated two-loop current and voltage PI control in Matlab/Simulink
 - Design firmware to regulate the output voltage to form 5V to 10V (in process)
- **Three-Phase Inverter Design** **Aug 2018 – Jan 2019**
 - Design isolated power supply and bootstrap circuit for gate driver
 - Design Op-Amp circuit for current sensing
- **Maximum Torque per Ampere (MTPA) Control of IPMSM** **Aug 2018 – Jan 2019**
 - Simulated the MTPA Control algorithm in MATLAB and Ansys Maxwell
 - Implemented Field Oriented Control (FOC) and hysteresis control in TI's DSP (C2000)
 - Design PI Controller for Current Control
 - Implemented MTPA in TI's DSP

LANGUAGE

Mandarin Chinese (Native Speaker)

English (Fluent)